A Possible Pathway for Rapid Growth of Sulfate during Haze Days in China

Guohui Li[1*], Naifang Bei[2], Junji Cao[1*], Rujin Huang[1*], Jiarui Wu[1], Tian Feng[1, 2], Yichen Wang[1], Suixin Liu[1], Qiang Zhang[3], Xuexi Tie[1], and Luisa T. Molina[4]

[1]Key Lab of Aerosol Chemistry and Physics, SKLLQG, Institute of Earth Environment, Chinese Academy of Sciences, Xi'an, China
[2]School of Human Settlements and Civil Engineering, Xi'an Jiaotong University, Xi'an, Shaanxi, China
[3]Department of Environmental Sciences and Engineering, Tsinghua University, Beijing, China
[4]Molina Center for Energy and the Environment, La Jolla, CA, and Massachusetts Institute of Technology, Cambridge, MA, USA
[*]Correspondence to: Guohui Li (ligh@ieecas.cn), Junji Cao (jjcao@ieecas.cn), and Rujin Huang (Rujin.Huang@psi.ch)

Abstract: Rapid industrialization and urbanization have caused frequent occurrence of haze in China during wintertime in recent years. The sulfate aerosol is one of the most important components of fine particles ($PM_{2.5}$) in the atmosphere, contributing significantly to the haze formation. However, the heterogeneous formation mechanism of sulfate remains poorly characterized. The relationships of the observed sulfate with $PM_{2.5}$, iron, and relative humidity in Xi'an, China have been employed to evaluate the mechanism and to develop a parameterization of the sulfate heterogeneous formation involving aerosol water for incorporation into atmospheric chemical transport models. Model simulations with the proposed parameterization can successfully reproduce the observed sulfate rapid growth and diurnal variations in Xi'an and Beijing, China. Reasonable representation of sulfate heterogeneous formation in chemical transport models considerably improves the $PM_{2.5}$ simulations, providing the underlying basis for better understanding the haze formation and supporting the design and implementation of emission control strategies.

1 Introduction

Sulfate is a main component of aerosols or fine particles ($PM_{2.5}$) in the atmosphere and plays a key role in global climate change. The direct and indirect radiative effects induced by sulfate aerosols have constituted one of the major uncertainties in current assessments of climate change (IPCC, 2013). In addition, deposition of sulfate aerosols exerts deleterious impacts on ecosystems through acidification of soils, lakes, and marshes (e.g., Schindler, 1988; Gerhardsson et al., 1994). Sulfate is also an important contributor to the haze formation and substantially reduces the atmospheric visibility during hazy days (e.g., He et al., 2014; Guo et al., 2014).

The main source of sulfate in the atmosphere is the oxidation of sulfur dioxide (SO_2), which is directly emitted from fossil fuel combustion, industrial processes, and volcanoes, or generated by oxidation of other sulfur-containing species, such as dimethyl sulfide (DMS). The conversion of SO_2 to sulfate involves various processes, including gas-phase oxidations by hydroxyl radicals (OH) and stabilized criegee intermediates (sCI) (Mauldin III et al., 2012), aqueous reactions in cloud or fog droplets, and heterogeneous reactions associated with aerosols (Seinfeld and Pandis, 2006).

Model studies have been performed to investigate the formation of sulfate aerosols on global or regional scales (Barrie et al., 2001). Previous global model results, considering the contribution of SO_2 gas-phase oxidation and aqueous reactions in cloud or fog droplets driven by ozone (O_3) and hydrogen peroxide (H_2O_2), have suggested that SO_2 mixing ratios are generally overestimated while sulfate concentrations tend to be underestimated, indicating that the two SO_2 oxidation pathways still cannot close the gap between field observations and modeling studies (Kasibhatla et al., 1997; Laskin et al., 2003). Incorporation of aqueous SO_2 oxidation by oxygen catalyzed by transition metal ions in models has improved sulfate simulations compared to measurements (Jacob and Hoffmann, 1983; Jacob et al., 1984, 1989;

Pandis and Seinfeld, 1992; Alexander et al., 2009), and recent studies have further shown the enhanced role of transition metal ions catalysis during in-cloud oxidation of SO_2 (Harris et al., 2013). However, models still underestimate SO_2 oxidation in winter source regions due to lack of cloud or fog or a missing oxidation mechanism (Feichter et al., 1996; Kasibhatla et al., 1997; Barrie et al., 2001). Therefore, heterogeneous conversion of SO_2 to sulfate associated with aerosols provides a possible pathway for improving the sulfate simulations in chemical transport models (CTMs) (Kasibhatla et al., 1997; Zhang et al., 2015).

Many experimental studies have been conducted to investigate the heterogeneous reactions of SO_2 on various oxides and mineral dust, but the underlying sulfate formation mechanism is still not comprehensively understood. Generally, the complicated sulfate heterogeneous formation from SO_2 is parameterized as a first-order irreversible uptake by aerosols in CTMs, with a reactive uptake coefficient ranging from 10^{-4} to 0.1 and also heavily depending on relative humidity in the atmosphere (Wang et al., 2014). It is still imperative to develop a ubiquitous parameterization of the SO_2 heterogeneous reaction to reasonably represent sulfate formation in CTMs.

In recent years, China has experienced frequently severe and persistent haze pollutions caused by elevated $PM_{2.5}$ concentrations, and field measurements have shown that sulfate aerosols are one of the most important species in $PM_{2.5}$ (He et al., 2014; Tian et al., 2016). Reasonable representation of sulfate aerosols provides underlying basis for $PM_{2.5}$ simulations. Laboratory experiments, field measurements, and model simulations have significantly advanced our understanding of SO_2 heterogeneous reactions in the atmosphere, providing a good opportunity to develop a parameterization to more reasonably represent the sulfate formation in CTMs. In this study, a parameterization for sulfate formation from SO_2 heterogeneous reactions has been developed based on the daily filter measurements in Xi'an since 2003, and verified using the Weather Research and Forecast model with Chemistry

(WRF-CHEM) in Xi'an and Beijing, China.

2 Model and Methodology

2.1 WRF-CHEM Model

In the present study, a specific version of the WRF-CHEM model (Grell et al., 2005) is utilized to assess the proposed heterogeneous sulfate parameterization, which is developed by Li et al. (2010, 2011a, b, 2012) at the Molina Center for Energy and the Environment. A new flexible gas phase chemical module is incorporated into the model to consider different chemical mechanisms, and the CMAQ/Models3 aerosol module developed by US EPA is adopted for aerosol simulations. Chemical species surface dry depositions are parameterized following Wesely (1989), and the wet deposition is calculated using the method in the CMAQ. The photolysis rates are calculated using the FTUV in which the aerosol and cloud effects on photolysis are included (Li et al., 2005; Li et al., 2011a).

The ISORROPIA Version 1.7 (Nenes et al., 1998) is used to predict inorganic aerosols in the WRF-CHEM model. A non-traditional SOA module is employed to calculate secondary organic aerosol (SOA) formation, including the volatility basis-set (VBS) modeling method in which primary organic components are assumed to be semi-volatile and photochemically reactive and are distributed in logarithmically spaced volatility bins. The SOA contributions from glyoxal and methylglyoxal are also considered as a first-order irreversible uptake by aerosol particles and cloud droplets in the model. Detailed information can be found in Li et al. (2011b).

Two persistent heavy haze pollution episodes are selected in the present study: (1) December 16 to 27, 2013 in the Guanzhong basin (GZB); and (2) January 13 to 21, 2014 in Beijing-Tianjin-Hebei (BTH) (Figure 1). Detailed model configurations and aerosol species observation sites are given in Table 1. A very severe haze episode occurred in GZB during the period from December 16 to 27, 2013, with an average $PM_{2.5}$ concentration of 325.6 μg m^{-3}. The maximum of the average $PM_{2.5}$ concentration in GZB even exceeded 500 μg m^{-3} during the episode. The average temperature and relative humidity in Xi'an was 3.7 °C and 72% during the episode, respectively, and the average wind speed was around 3.7 m s^{-1}. The average $PM_{2.5}$ concentration from January 13 to 21, 2014 in BTH was 195.3 μg m^{-3}, with a maximum of 363.9 μg m^{-3}. The average temperature and relative humidity in Beijing during the episode was -0.5 °C and 42%, respectively, and the average wind speed was about 7.4 m s^{-1}.

2.2 Statistical Methods for Comparisons

The mean bias (*MB*) and the index of agreement (*IOA*) are used to evaluate the performance of the WRF-CHEM model in simulating gas-phase species and aerosols against measurements. The *IOA* varies from 0 to 1, with 1 indicating perfect agreement of the prediction with the observation.

$$MB = \frac{1}{N}\sum_{i=1}^{N}(P_i - O_i)$$

$$IOA = 1 - \frac{\sum_{i=1}^{N}(P_i - O_i)^2}{\sum_{i=1}^{N}(|P_i - \bar{O}| + |O_i - \bar{O}|)^2}$$

where P_i and O_i are the calculated and observed pollutant concentrations, respectively. N is the total number of the predictions used for comparisons, and $\bar{P}$ and $\bar{O}$ represents the average of the prediction and observation, respectively.

2.3 Pollutants Measurements

The hourly near-surface NO_2, SO_2, and $PM_{2.5}$ mass concentrations in GZB and BTH are released by the China's Ministry of Environmental Protection (China MEP) and can be downloaded from the website http://www.aqistudy.cn/. The daily filter measurements of aerosol species have been performed since 2003 at the Institute of Earth Environment, Chinese Academy of Sciences (hereafter referred to as IEECAS, 34.23°N, 108.88°E) in Xi'an, China (Figure 1a). The sulfate, nitrate, ammonium, and organic aerosols are measured by the Aerodyne High Resolution Time-of-Flight Aerosol Mass Spectrometer (HR-ToF-AMS) with a novel $PM_{2.5}$ lens from 13 December 2013 to 6 January 2014 at IEECAS site in Xi'an and from 9 to 26 January 2014 at the Institute of Remote Sensing and Digital Earth, Chinese Academy of Sciences (40.00°N, 116.38°E) in Beijing (Figure 1b). Detailed information about the HR-ToF-AMS measurement can be found in Elser et al. (2016).

3 Results and Discussions

3.1 Parameterization of SO_2 Heterogeneous Reaction Involving Aerosol Water

Figure 2 shows the scatter plot of the wintertime sulfate and $PM_{2.5}$ daily mass concentrations at IEECAS from 2003 to 2010. The wintertime is defined as December of the year to February of the next year. The observed daily $PM_{2.5}$ mass concentrations frequently exceed 150 μg m^{-3} during wintertime, showing that Xi'an has experienced heavy air pollution. The sulfate aerosols constitute about 15.7% of the $PM_{2.5}$ mass concentration on average, and the occurrence frequency with the daily sulfate mass concentration exceeding 50 μg m^{-3} is around 25.7%.

The observed high level of sulfate aerosols is hardly interpreted using SO_2 gas-phase oxidations by OH and sCI due to the low O_3 level in the winter. The insolation is weak during wintertime in North China, unfavorable for photochemical activities. The O_3 formation is slow and the observed O_3 concentrations are very low, particularly during haze episodes. The real-time hourly measurements of O_3 and $PM_{2.5}$ concentrations during 2013 and 2015 wintertime are analyzed as follows in GZB (5 cities, 39 sites, Figure 1a), which are released by China MEP since 2013. Values of the hourly $PM_{2.5}$ concentrations ($[PM_{2.5}]$) are first subdivided into 20 bins with the interval of 25 μg m^{-3}. O_3 concentrations ($[O_3]$) in the 5 cities as $[PM_{2.5}]$ are assembled, and an average of $[O_3]$ in each bin are calculated (Nakajima et al., 2001; Kawamoto et al., 2006). As shown in Figure 3, when [$PM_{2.5}$] increase from 10 to 75 μg m^{-3}, [O_3] significantly decrease from around 41 to 23 μg m^{-3}; when [$PM_{2.5}$] exceed 200 μg m^{-3}, [O_3] fluctuate between 18 and 21 μg m^{-3}. The average [O_3] in the 5 cities during the 2013 and 2015 wintertime are 27 μg m^{-3} (about 13.5 ppbv). Considering the determining role of O_3 in the formation of OH and sCI in the atmosphere, the very low level of [O_3] during wintertime significantly reduces the efficiency of the sulfate formation from SO_2 oxidation by OH and sCI.

Humid conditions have been observed to facilitate the sulfate formation in the atmosphere (e.g., Sun et al., 2013; Zheng et al., 2015). Figure 4 presents the scatter plot of the wintertime sulfate at IEECAS and the relative humidity (RH) at an adjacent meteorological station from 2003 to 2010. The observed sulfate displays a positive correlation with the RH with the correlation coefficient of 0.70, indicating that the aerosol water induced by the aerosol wet growth might play an important role in the sulfate formation. It is worthy to note that since high RH often coincides with stagnation, the concentrations of a lot of pollutants also build up during high RH periods. There are two possible pathways for the sulfate formation: bulk aqueous-phase oxidation of SO_2 in aerosol water and heterogeneous reaction of SO_2 on aerosol surfaces involving aerosol water.

The heterogeneous reaction of SO_2 on dust surfaces has been investigated comprehensively, but the sulfate formation mechanism is still not completely understood. Possible mechanisms have been proposed that mineral dust and NO_2 enhance the conversion of SO_2 to sulfate (He et al., 2014; Xie et al., 2015; Xue et al., 2016). Size-segregated particle samples in Beijing have shown that a considerable amount of sulfate is distributed in the coarse mode with particle diameters ranging from 2.1 to 9 μm, but sulfate peak concentrations still occur in the fine mode with particle diameters ranging from 0.43 to 1.1 μm (Tian et al., 2016). Oxidation of sulfite by NO_2 in aerosol water has also been proposed to contribute considerably to the sulfate production when NH_3 concentrations are sufficiently high (Pandis and Seifeld, 1989; Xie et al., 2015).

Laboratory or field studies have suggested that O_3 or Fe^{3+} can oxidize sulfite to sulfate. Considering the low $[O_3]$ during wintertime (Figure 3), the oxidation of sulfite by O_3 cannot constitute the main source of the wintertime sulfate. Mineral dust and coal combustion in China could provide sufficient iron. Measurements have indicated that mineral dust accounts for about 10% of $PM_{2.5}$ in Beijing (He et al., 2014). Observations at an urban site in Ji'nan, China have also shown enhanced iron concentrations during haze episodes, ranging from 0.7 to 5.5 $\mu g\ m^{-3}$, which are primarily emitted from steel smelting and coal combustion (Wang et al., 2012). Figure 5 shows the scatter plot of the wintertime $PM_{2.5}$ and iron at IEECAS site from 2003 to 2010. The iron mass concentration generally increases with $[PM_{2.5}]$, varying from 0.1 to 10 $\mu g\ m^{-3}$, but does not correlate well with the $[PM_{2.5}]$ with the correlation coefficient of 0.34, showing considerable background iron contributions. We assume that 1% of iron in Xi'an is dissolved in aerosol water and 1% of dissolved iron is in the Fe^{3+} oxidation state (Alexander et al., 2009). When the aerosol water concentration varies from 100 to 1000 $\mu g\ m^{-3}$, the Fe^{3+} concentrations in Xi'an are between 0.18 and 180 μM, providing favorable conditions for the oxidation of adsorbed sulfite (Seinfeld and Pandis, 2006).

We propose here a SO_2 heterogeneous reaction parameterization in which the SO_2 oxidation in aerosol water by O_2 catalyzed by Fe^{3+} is limited by mass transfer resistances in the gas-phase and the gas-particle interface.

$$S(IV) + \frac{1}{2}O_2 \xrightarrow{Fe^{3+}} S(VI)$$

When the solution pH is between 5.0 and 7.0, the oxidation reaction is second order in dissolved iron and first order in S(IV) and can be expressed as follows (Seinfeld and Pandis, 2006):

$$-\frac{d[S(IV)]}{dt} = 1\times10^{-3}[S(IV)] \quad 5.0 < pH < 6.0$$

$$-\frac{d[S(IV)]}{dt} = 1\times10^{-4}[S(IV)] \quad pH \sim 7.0$$

where [S(IV)] is the sulfite (S(IV)) concentration. The measured SO_2 mass accommodation coefficient on aqueous surfaces is around 0.1 (Worsnop et al., 1989). Due to sufficient NH_3 and presence of mineral dust in the atmosphere in North China, the calculated pH in aerosol water is between 5.0 and 7.0 (Cao et al., 2013). The SO_2 uptake coefficient on aerosol water surface is estimated to be about $10^{-4} \sim 10^{-5}$ if the sulfite oxidation is catalyzed by Fe^{3+}. The sulfate heterogeneous formation from SO_2 is therefore parameterized as a first-order irreversible uptake by aerosols, with a reactive uptake coefficient of 0.5×10^{-4}, assuming that there is enough alkalinity to maintain the high iron-catalyzed reaction rate:

$$\frac{d[SO_2]}{dt} = -\left(\frac{1}{4}\gamma_{SO_2}\upsilon_{SO_2}A_w\right)[SO_2]$$

where $[SO_2]$ is the SO_2 concentration, A_w is the aerosol water surface area, γ_{SO_2} is the SO_2 reactive uptake coefficient, and υ_{SO_2} is the SO_2 thermal velocity. The aerosol hygroscopic growth is directly predicted by ISORROPIA (Version 1.7) in the model and the aerosol water surface area is scaled from the calculated wet aerosol surface area using the third-moment of aerosol species. Considering that O_3 and NO_2 also play a considerable role in the sulfite oxidation when pH is high (Pandis and Seinfeld, 1989), future studies are needed to consider the O_3 and NO_2 contribution to the sulfate formation.

A box model is devised to interpret the rapid growth of sulfate observed at IEECAS site during 2013 wintertime in Xi'an. In this model, the proposed heterogeneous reaction of SO_2 involving aerosol water (hereafter referred to as $HRSO_2$) parameterization is included and ISORROPIA (Version 1.7) is used to simulate sulfate, nitrate, ammonium aerosols, and aerosol water. In addition, inorganic aerosols are represented by a two-moment modal approach with a lognormal size distribution. A severe haze episode occurred from December 16 to 25, 2013 in GZB, with the average observed $[PM_{2.5}]$ exceeding 400 μg m^{-3} during the period from December 23 to 25, 2013. The HR-ToF-AMS measured sulfate concentrations reaching about 250 μg m^{-3} in the morning on December 23, and particularly, the observed sulfate concentration increased from 132 μg m^{-3} at 07:30 BJT to 240 μg m^{-3} at 09:30 BJT. The box model is utilized to simulate the rapid sulfate growth from 07:30 to 09:30 BJT, constrained by the observed temperature, SO_2, nitrate, and ammonium (Table 2). There was no RH observation at the IEECAS site; the observed RH at adjacent meteorological stations ranged from 93% to 99% during the time period. In addition, the atmosphere was calm and stable during the simulation period due to the control of a high pressure system over GZB, so the horizontal transport is not considered. Various RHs from 93% to 99% are used to calculate the sulfate growth in the box model. Figure 6 shows the calculated and observed sulfate concentrations from 07:30 to 09:30 on December 23, 2013. The RH significantly influences the sulfate formation and the sulfate concentrations increase nonlinearly with the RH. When the RH is 93%, the sulfate concentration is increased by 22.7 μg m^{-3} after 2-hour integration, whereas the enhanced sulfate concentration reaches 216.6 μg m^{-3} when the RH is 99%. The simulated sulfate concentrations are best fit for the observation when the RH is 98%. It is worth noting that, when RH is high (i.e., exceeding 95% or so), there is always the possibility of the presence of fog. Studies have demonstrated that for every observed sulfate peak in the 1980s in Los Angeles, there is fog present (Pandis and Seinfeld, 1989; Pandis et al., 1992). Hence, the box model simulations with the RH ranging from 93% to 99% strongly suggest that there was at least some patchy fog in the area, which would provide sufficient water for the rapid iron-catalyzed reaction. Further studies need to be performed to investigate the possible contributions of the patchy fog on the sulfate formation.

3.2 Sulfate Simulations in GZB and BTH

The proposed $HRSO_2$ parameterization is further incorporated into the WRF-CHEM model to simulate sulfate aerosols. Two simulations are performed for GZB and BTH respectively, including the base case (hereafter referred to as B-case) without the HRSO$_2$ parameterization and the enhanced oxidation case (hereafter referred to as E-case) with the HRSO$_2$ parameterization. In Figures 7 and 8, we present the spatial distributions of calculated and observed near-surface [PM$_{2.5}$] at 00:00 BJT in the E-case on selected six days representing the haze development in GZB and BTH, respectively, along with the simulated wind fields. In general, the predicted PM$_{2.5}$ spatial patterns agree well with the observations at the ambient monitoring sites in GZB and BTH. The model reproduces well the high [PM$_{2.5}$] in GZB, although it tends to underestimate the observation in the west of GZB. Due to the specific topography, when the northeast winds are prevalent in GZB, pollutants tend to accumulate, and simulated and observed [PM$_{2.5}$] can be up to 500 μg m^{-3}. When the north winds are intensified on 26 December 2013, the pollutants commence to be transported outside of GZB. In BTH, simulated weak winds cause severe PM$_{2.5}$ pollutions, with [PM$_{2.5}$] frequently exceeding 250 μg m^{-3} at most of areas of BTH, which is consistent with the observations over monitoring sites. Hence, in general, the model reasonably well reproduces the haze formation in GZB and BTH.

In the present study, ISORROPIA (Version 1.7) is employed to predict the thermodynamic equilibrium between the sulfate-nitrate-ammonium-water aerosols and their gas phase precursors H_2SO_4-HNO_3-NH_3-water vapor. SO$_2$ and NO$_2$ are the precursors of H_2SO_4 and HNO_3, so it is imperative to evaluate the SO$_2$ and NO$_2$ simulations using the measurements to more reasonably calculate inorganic aerosols concentrations.

Figures 9 and 10 show the temporal profiles of observed and simulated near-surface [NO$_2$] and [SO$_2$] averaged over monitoring sites in GZB from December 16 to 27, 2013 and in BTH from January 13 to 21, 2014, respectively. The model performs well in simulating the [NO$_2$] temporal variations compared with observations in GZB and BTH, both with the *IOA* of 0.91 in the E-case. The difference of the simulated [NO$_2$] in the B-case and E-case is minor, and the average [NO_2] is increased by 0.69% in GZB and decreased by 0.1% in BTH in the E-case compared to the B-case, showing that the impact of the $HRSO_2$ parameterization on NO_2 simulations is not significant in GZB and BTH. Although the model replicates the temporal variations of [SO_2] compared to the measurements in GZB and NCP in the E-case with *IOAs* of around 0.80, the model biases still exist. The model generally underestimates [SO_2] in GZB and BTH, with *MBs* of -3.4 μg m^{-3} and -0.8 μg m^{-3}. One of the possible reasons for SO_2 simulation biases is that large amounts of SO_2 are emitted from point sources, such as power plants or agglomerated industrial zones, and the transport of SO_2 from point sources is more sensitive to the wind field simulation uncertainties (Bei et al., 2012). The $HRSO_2$ parameterization generally improves the SO_2 simulations by accelerating SO_2 conversions to sulfate, decreasing the *MB* from 11.0 μg m^{-3} in the B-case to -3.4 μg m^{-3} in the E-case in GZB and 5.0 μg m^{-3} in the B-case to -0.8 μg m^{-3} in the E-case in BTH. On average, inclusion of the $HRSO_2$ parameterization decreases the [SO_2] by 15.9% and 3.4% in GZB and BTH on average, respectively. Overall, the model performs well in simulating the NO_2 and SO_2 temporal variations against the measurements in GZB and BTH in the E-case. Due to lack of routine measurements of NH_3 in GZB and BTH, the evaluation of the model performance on NH_3 is not provided in the present study. Future studies are imperative to be performed to evaluate the model performance on NH_3 which plays an important role in the sulfate formation (Wang et al., 2017).

Figures 11 and 12 display the simulated and observed inorganic aerosol variations in Xi'an from December 16 to 27, 2013 and in Beijing from January 13 to 21, 2014, respectively. In Xi'an, the observed sulfate mass concentrations range from 50 to 250 μg m^{-3}, constituting the second most important $PM_{2.5}$ component during the episode. The $HRSO_2$ parameterization substantially improves the sulfate simulations in the E-case compared to those in the B-case against the measurements. In the B-case, the sulfate concentrations are remarkably underestimated, with a *MB* of -72.4 μg m^{-3} (Table 3). However, in the E-case, the WRF-CHEM model generally yields the observed sulfate variations during the 11-day episode, with a MB of -17.0 μg m^{-3} and an IOA of 0.89, and the average sulfate concentration is enhanced by 172% compared to the B-case. In Beijing, the model also reproduces the observed sulfate variations reasonably well during the 7-day episode in the E-case, with a *MB* of -0.8 μg m^{-3} and an *IOA* of 0.88 (Table 3), but cannot adequately predict the observed sulfate peaks. The average sulfate concentration is enhanced by 58.4% in the E-case compared to the B-case in Beijing. The improvement of sulfate simulations caused by the HRSO$_2$ parameterization in Beijing is not as obvious as that in Xi'an due to the very humid conditions in GZB during the simulation period, which facilitate the rapid conversion of SO$_2$ to sulfate and cause the SO$_2$ heterogeneous conversion to be the dominant sulfate source.

Considering the importance of RH in the SO$_2$ heterogeneous oxidation, Figure 13 shows the simulated and observed RH diurnal profiles in Xi'an from December 16 to 27, 2013 and in Beijing from January 13 to 21, 2014. The model generally performs reasonably well in simulating the observed RH, with *IOAs* of 0.80 for Xi'an and 0.76 for Beijing. Overall, the model is subject to overestimate the RH, especially in Beijing, but well captures the observed peaks of the RH in Beijing and Xi'an. The RH biases considerably affect the sulfate simulations. The underestimation of the high RH generally corresponds the underestimation of the sulfate concentration, i.e., during nighttime on January 15 and 16, 2014 in Beijing, and in the morning from December 23 to 25, 2013 in Xian. It is worthy to note that during the two episodes, the SO$_2$ oxidation by OH to the sulfate formation is not important. We have performed additional sensitivity simulations in which only the direct emissions of sulfate are considered. Comparisons of the sensitivity simulation with the B-case show that the SO$_2$ oxidation by OH can explain about 5.1% and 11.7% of the observed sulfate concentrations in Xi'an and Beijing on average, respectively.

Although the *IOA* for nitrate aerosols is 0.83, the nitrate underestimation is rather large from 17 to 21 December 2013 in Xi'an in the E-case. The nitrate simulations are improved in Beijing compared to those in Xi'an, with a *MB* of -4.2 μg m^{-3} and an *IOA* of 0.88 in the E-case. The nitrate simulations in the B-case are slightly better than those in the E-case, caused by the underestimation of sulfate aerosols in the B-case, which is favorable for more HNO_3 to exist in the aerosol phase. The inclusion of the $HRSO_2$ parameterization deceases the simulated nitrate concentration by 15.3% and 19.5% in Xi'an and Beijing, respectively, on average. The model performs well in predicting the ammonium aerosols in Xi'an and Beijing, with *IOAs* of around 0.90 in the E-case. The ammonium simulations in the E-case are improved compared to those in the B-case against the measurement, showing that sulfate aerosols play an important role in the ammonium aerosol formation. The average ammonium concentration is enhanced by 36.8% in Xi'an and 7.2% in Beijing by the inclusion of the $HRSO_2$ parameterization. Considering the substantial influence of simulated meteorological fields uncertainties on the aerosol species comparison at a single site (Bei et al., 2012), the $HRSO_2$ parameterization performs reasonably well in simulating the observed inorganic aerosol variations in Xi'an and Beijing in the E-case.

Recently, Wang et al., (2016) have also elucidated a specific mechanism for the sulfite-sulfate conversion, in which oxidation of sulfite by NO_2 in aerosol water in case of high NH_3 concentrations contributes considerably to the sulfate production. They have also pointed out the critical role of the sulfate formation in haze formation in China through further promoting the formation of SOA and nitrate due to the enhanced hygroscopicity. Zhang et al. (1995) have reported that the high concentration of nitrate is attributed to an efficient heterogeneous conversion of NO_x to HNO_3 due to the hydrolysis of N_2O_5 on sulfate aerosols. Zhao et al. (2006) have investigated the heterogeneous chemistry of methylglyoxal with liquid H_2SO_4, showing that the hydration and oligomerization reactions of methylglyoxal are enhanced by sulfate formation due to the high dependence of these reactions on particle hygroscopicity. Therefore, future studies need to be performed to incorporate the specific mechanism into CTMs to improve sulfate, nitrate, and SOA simulations.

Figure 14 presents the observed and simulated diurnal cycles of mass concentrations of NO_2 and SO_2 averaged over GZB and BTH and the sulfate, nitrate, and ammonium aerosols in Xi'an and Beijing during the simulated episodes. The WRF-CHEM model performs well in simulating the NO_2 diurnal cycles compared to measurements over GZB and BTH in the E-case. The model also reasonably reproduces the observed diurnal cycles of SO_2 over GZB, sulfate, nitrate, and ammonium aerosols in Xi'an in the E-case, particularly the sulfate simulations are significantly improved in the E-case compared with the B-case against the measurements. However, the model does not predict well the observed diurnal cycles of sulfate, nitrate, and ammonium aerosols in Beijing, showing the model biases in simulating the south or east wind fronts.

As one of the most important components of $PM_{2.5}$, reasonable representation of sulfate heterogeneous formation in CTMs is imperative to $PM_{2.5}$ simulations and predictions. Figure 15 presents the temporal profiles of observed and simulated near-surface [$PM_{2.5}$] averaged over monitoring sites in GZB from December 16 to 27, 2013 and in BTH from January 13 to 21, 2014, respectively. Inclusion of the $HRSO_2$ parameterization in the E-case improves the ability of the model to reproduce the $PM_{2.5}$ measurements in GZB and BTH. In GZB, due to very humid conditions which facilitate the heterogeneous sulfate formation during the episode, the simulated $PM_{2.5}$ mass concentrations are increased by more than 40 $\mu g\ m^{-3}$ in the E-case compared to the B-case with an average increase of 12.3%, and more consistent with the measurements. The $HRSO_2$ parameterization also improves the $PM_{2.5}$ simulations in BTH, with an average increase of less than 3.0%, reducing the underestimation from around -13.3 to -5.1 $\mu g\ m^{-3}$. The $HRSO_2$ parameterization enhances considerably the [$PM_{2.5}$] in GZB

(Figure 16a), with the average [$PM_{2.5}$] contribution of about 10 – 50 μg m^{-3} from December 16 to 27, 2013. The average [$PM_{2.5}$] contributions of the sulfate heterogeneous formation is around 2 – 30 μg m^{-3} in BTH (Figure 16b) from January 13 to 21, 2014, lower than those in GZB.

The sulfate aerosol significantly affects nitrate and ammonium formation in the atmosphere due to its stability and the deliberate thermodynamic equilibrium between inorganic aerosols and their precursors. The simulated hourly near-surface sulfate concentrations in E-case during the whole episode are first subdivided into 20 bins with the interval of 5 μg m^{-3}. Inorganic aerosols and $PM_{2.5}$ concentrations in the B-case and E-case as the bin sulfate concentrations in the E-case following the grid cells are assembled respectively, and an average of inorganic aerosols and $PM_{2.5}$ concentrations in each bin are calculated. Figures 17 and 18 show the impacts of the $HRSO_2$ parameterization on the inorganic aerosols and $PM_{2.5}$ simulations in GZB and NCP, respectively. The heterogeneous sulfate formation determines the sulfate level when the sulfate concentration in the E-case is more than 25 μg m^{-3}, with the contribution exceeding 50% in GZB. However, in BTH, the heterogeneous sulfate formation plays a more important role in the sulfate level only when the sulfate concentration in the E-case exceeds 45 μg m^{-3}. If the $HRSO_2$ parameterization is not considered, the model generally predicts more nitrate and less ammonium aerosols (Figures 17b-c and 18b-c). In addition, the [$PM_{2.5}$] contributions of the heterogeneous sulfate formation exceed 5% and 10% when the simulated sulfate concentrations in the E-case are more than 10 μg m^{-3} and 80 μg m^{-3} in GZB respectively (Figure 17d). However, in BTH, the contributions exceed 5% when the simulated sulfate concentrations in the E-case are higher than 50 μg m^{-3} (Figure 18d).

4 Summary and Conclusions

In the present study, a parameterization of sulfate heterogeneous formation involving aerosol water ($HRSO_2$) is developed based on the daily filter measurements in Xi'an since 2003. A SO_2 heterogeneous reaction parameterization has been proposed, in which the SO_2 oxidation in aerosol water by O_2 catalyzed by Fe^{3+} is limited by mass transfer resistances in the gas-phase and the gas-particle interface. The sulfate heterogeneous formation from SO_2 is parameterized as a first-order irreversible uptake by aerosol water surfaces, with a reactive uptake coefficient of 0.5×10^{-4} assuming that there is enough alkalinity to maintain the high iron-catalyzed reaction rate. A box model with the $HRSO_2$ parameterization successfully reproduces the observed rapid sulfate formation at IEECAS site in Xi'an.

The $HRSO_2$ parameterization is implemented into the WRF-CHEM model to simulate sulfate aerosols. Two persistent heavy haze pollution episodes are simulated with and without the SO_2 heterogeneous reaction: (1) December 16 to 27, 2013 in GZB, and (2) January 13 to 21, 2014 in BTH. In general, the model performs reasonably well in simulating the $PM_{2.5}$ distributions, the NO_2 and SO_2 temporal variations compared with observations in GZB and NCP. The $HRSO_2$ parameterization improves the SO_2 simulations by accelerating SO_2 conversions to sulfate aerosols.

The $HRSO_2$ parameterization substantially improves the sulfate simulations compared to the measurements in Xi'an and Beijing, particularly under humid conditions. In Xi'an, the sulfate concentrations are substantially underestimated when the $HRSO_2$ parameterization is not considered in the simulations. Inclusion of the $HRSO_2$ parameterization significantly enhances the sulfate formation, and the model generally produces the observed sulfate variations during the 11-day episode. In Beijing, improvement in sulfate simulations with $HRSO_2$ parameterization is not as obvious as that in Xi'an because of the very humid conditions in GZB during the simulation period. The $HRSO_2$ parameterization also improves the ammonium simulations in Xi'an and Beijing compared to observations, as well as appreciably improves the $PM_{2.5}$ simulations against the measurements over monitoring sites in GZB and NCP.

In summary, reasonable representation of sulfate heterogeneous formation not only improves the $PM_{2.5}$ simulations, but also helps rationally verify the contribution of inorganic aerosols to $PM_{2.5}$, providing the underlying basis for better understanding the haze formation and supporting the design and implementation of emission control strategies.

Data availability: The real-time NO_2, SO_2 and $PM_{2.5}$ are accessible for the public on the website http://106.37.208.233:20035/. The historic profile of observed ambient pollutants is also available at http://www.aqistudy.cn/.

Acknowledgements. The authors would like to acknowledge helpful discussion with Professor Spyros Pandis. This work was supported by the National Natural Science Foundation of China (No. 41275153) and supported by the "Strategic Priority Research Program" of the Chinese Academy of Sciences，Grant No. XDB05060500. Guohui Li is also supported by the "Hundred Talents Program" of the Chinese Academy of Sciences. Naifang Bei is supported by the National Natural Science Foundation of China (No. 41275101).

References

Alexander, B., Park, R. J., Jacob, D. J., and Gong, S. L.: Transition metal-catalyzed oxidation of atmospheric sulfur: Global implications for the sulfur budget, Journal of Geophysical Research-Atmospheres, 114, 13, 10.1029/2008jd010486, 2009.

Barrie, L. A., Yi, Y., Leaitch, W. R., Lohmann, U., Kasibhatla, P., Roelofs, G. J., Wilson, J., McGovern, F., Benkovitz, C., Melieres, M. A., Law, K., Prospero, J., Kritz, M., Bergmann, D., Bridgeman, C., Chin, M., Christensen, J., Easter, R., Feichter, J., Land, C., Jeuken, A., Kjellstrom, E., Koch, D., and Rasch, P.: A comparison of large-scale atmospheric sulphate aerosol models (COSAM): overview and highlights, Tellus Series B-Chemical and Physical Meteorology, 53, 615-645, 10.1034/j.1600-0889.2001.530507.x, 2001.

Bei, N., Li, G., and Molina, L. T.: Uncertainties in SOA simulations due to meteorological uncertainties in Mexico City during MILAGRO-2006 field campaign, Atmospheric Chemistry and Physics, 12, 11295-11308, 10.5194/acp-12-11295-2012, 2012.

Bei, N. F., Li, G. H., Huang, R. J., Cao, J. J., Meng, N., Feng, T., Liu, S. X., Zhang, T., Zhang, Q., and Molina, L. T.: Typical synoptic situations and their impacts on the wintertime air pollution in the Guanzhong basin, China, Atmospheric Chemistry and Physics, 16, 7373-7387, 10.5194/acp-16-7373-2016, 2016.

Cao, J., Tie, X., Dabberdt, W. F., Jie, T., Zhao, Z., An, Z., and Shen, Z.: On the potential high acid deposition in northeastern China, Journal of Geophysical Research-Atmospheres, 118, 4834-4846, doi:10.1002/jgrd.50381, 2013.

Chen, F., and Dudhia, J.: Coupling an advanced land surface-hydrology model with the Penn State-NCAR MM5 modeling system. Part I: Model implementation and sensitivity, Mon. Weather Rev., 129, 569-585, 10.1175/1520-0493(2001)129<0569:caalsh>2.0.co;2, 2001.

Chen, W., Yan, L., and Zhao, H. M.: Seasonal Variations of Atmospheric Pollution and Air Elser, M., Huang, R.-J., Wolf, R., Slowik, J. G., Wang, Q., Canonaco, F., Li, G., Bozzetti, C., Daellenbach, K. R., Huang, Y., Zhang, R., Li, Z., Cao, J., Baltensperger, U., El-Haddad, I., and Prévôt, A. S. H.: New insights into $PM_{2.5}$ chemical composition and sources in two major cities in China during extreme haze events using aerosol mass spectrometry, Atmospheric Chemistry and Physics, 16, 3207-3225, doi:10.5194/acp-16-3207-2016, 2016.

Chou, M.-D. and M. J. Suarez: A solar radiation parameterization for atmospheric studies, NASA Tech. Rep. NASA/TM-1999-10460, 15, 38 pp, 1999.

Chou, M.-D. and M. J. Suarez: A thermal infrared radiation parameterization for atmospheric studies, NASA/TM-2001-104606, 19, 55 pp, 2001.

Feichter, J., Kjellstrom, E., Rodhe, H., Dentener, F., Lelieveld, J., and Roelofs, G. J.: Simulation of the tropospheric sulfur cycle in a global climate model, Atmospheric Environment, 30, 1693-1707, 10.1016/1352-2310(95)00394-0, 1996.

Gerhardsson, L., Oskarsson, A., and Skerfving, S.: Acid precipitation effects on trace-elements and human health, Science of Total Environment, 153, 237-245, 10.1016/0048-9697(94)90203-8, 1994.

Grell, G., and Baklanov, A.: Integrated modeling for forecasting weather and air quality: A call for fully coupled approaches, Atmospheric Environment, 45, 6845-6851, 10.1016/j.atmosenv.2011.01.017, 2011.

Guo, S., Hu, M., Zamora, M. L., Peng, J. F., Shang, D. J., Zheng, J., Du, Z. F., Wu, Z., Shao, M., Zeng, L. M., Molina, M. J., and Zhang, R. Y.: Elucidating severe urban haze formation in China, Proceedings of the National Academy of Sciences of the United States of America, 111, 17373-17378, 10.1073/pnas.1419604111, 2014.

Guenther, A., Karl, T., Harley, P., Wiedinmyer, C., Palmer, P. I., and Geron, C.: Estimates of global terrestrial isoprene emissions using MEGAN (Model of Emissions of Gases and Aerosols from Nature), Atmospheric Chemistry and Physics, 6, 3181-3210, 2006.

Harris, E., Sinha, B., van Pinxteren, D., Tilgner, A., Fomba, K. W., Schneider, J., Roth, A., Gnauk, T., Fahlbusch, B., Mertes, S., Lee, T., Collett, J., Foley, S., Borrmann, S., Hoppe, P., and Herrmann, H.: Enhanced role of transition metal ion catalysis during in-cloud oxidation of SO_2, Science, 340, 2013.

He, H., Wang, Y. S., Ma, Q. X., Ma, J. Z., Chu, B. W., Ji, D. S., Tang, G. Q., Liu, C., Zhang, H. X., and Hao, J. M.: Mineral dust and NO_x promote the conversion of SO_2 to sulfate in heavy pollution days, Scientific Report, 4, 5, 10.1038/srep04172, 2014.

Hong, S.-Y., and Lim, J.-O. J.: The WRF Single-Moment 6-Class Microphysics Scheme (WSM6), Asia-Pacific Journal of Atmospheric Sciences, 42, 129-151, 2006.

Horowitz, L. W., Walters, S., Mauzerall, D. L., Emmons, L. K., Rasch, P. J., Granier, C., Tie, X. X., Lamarque, J. F., Schultz, M. G., Tyndall, G. S., Orlando, J. J., and Brasseur, G. P.: A global simulation of tropospheric ozone and related tracers: Description and evaluation of MOZART, version 2, Journal of Geophysical Research-Atmospheres, 108, 29, 10.1029/2002jd002853, 2003.

Jacob, D. J., and Hoffmann, M. R.: A dynamic model for the production of H^+, NO_3^-, and SO_4^{2-} in urban fog, Journal of Geophysical Research-Oceans and Atmospheres, 88, 6611-6621, 10.1029/JC088iC11p06611, 1983.

Jacob, D. J., Waldman, J. M., Munger, J. W., and Hoffmann, M. R.: A field investigation of physical and chemical mechanisms affecting pollutant concentrations in fog droplets, Tellus Series B-Chemical and Physical Meteorology, 36, 272-285, 1984.

Jacob, D. J., Gottlieb, E. W., and Prather, M. J.: Chemistry of a polluted cloudy boundary-layer, Journal of Geophysical Research-Atmospheres, 94, 12975-13002, 10.1029/JD094iD10p12975, 1989.

Janjić, Z. I.: Nonsingular Implementation of the Mellor–Yamada Level 2.5 Scheme in the NCEP Meso Model, Ncep Office Note, 436, 2002.

Kasibhatla, P., Chameides, W. L., and StJohn, J.: A three-dimensional global model investigation of seasonal variations in the atmospheric burden of anthropogenic sulfate aerosols, Journal of Geophysical Research-Atmospheres, 102, 3737-3759, 10.1029/96jd03084, 1997.

Kawamoto, K., Hayasaka, T., Uno, I., and Ohara, T.: A correlative study on the relationship between modeled anthropogenic aerosol concentration and satellite-observed cloud properties over east Asia, Journal of Geophysical Research-Atmospheres, 111, 7, 10.1029/2005jd006919, 2006.

Laskin, A., Gaspar, D. J., Wang, W. H., Hunt, S. W., Cowin, J. P., Colson, S. D., and Finlayson-Pitts, B. J.: Reactions at interfaces as a source of sulfate formation in sea-salt particles, Science, 301, 340-344, 10.1126/science.1085374, 2003.

Li, G., Zhang, R., Fan, J., and Tie, X.: Impacts of black carbon aerosol on photolysis and ozone, Journal of Geophysical Research, 110, 10.1029/2005jd005898, 2005.

Li, G., Lei, W., Zavala, M., Volkamer, R., Dusanter, S., Stevens, P., and Molina, L. T.: Impacts of HONO sources on the photochemistry in Mexico City during the MCMA-2006/MILAGO Campaign, Atmospheric Chemistry and Physics, 10, 6551-6567, 10.5194/acp-10-6551-2010, 2010.

Li, G., Bei, N., Tie, X., and Molina, L. T.: Aerosol effects on the photochemistry in Mexico City during MCMA-2006/MILAGRO campaign, Atmospheric Chemistry and Physics, 11, 5169-5182, 10.5194/acp-11-5169-2011, 2011a.

Li, G., Zavala, M., Lei, W., Tsimpidi, A. P., Karydis, V. A., Pandis, S. N., Canagaratna, M. R., and Molina, L. T.: Simulations of organic aerosol concentrations in Mexico City using the WRF-CHEM model during the MCMA-2006/MILAGRO campaign, Atmospheric Chemistry and Physics, 11, 3789-3809, 10.5194/acp-11-3789-2011, 2011b.

Li, G., Lei, W., Bei, N., and Molina, L. T.: Contribution of garbage burning to chloride and $PM_{2.5}$ in Mexico City, Atmospheric Chemistry and Physics, 12, 8751-8761, 10.5194/acp-12-8751-2012, 2012.

Martin, L. R., and Hill, M. W.: The effect of ionic-strength on the manganese catalyzed oxidation of sulfur(iv), Atmospheric Environment, 21, 2267-2270, 1987.

Mauldin, R. L., Berndt, T., Sipila, M., Paasonen, P., Petaja, T., Kim, S., Kurten, T., Stratmann, F., Kerminen, V. M., and Kulmala, M.: A new atmospherically relevant oxidant of sulphur dioxide, Nature, 488, 193-196, 10.1038/nature11278, 2012.

Nakajima, T., Higurashi, A., Kawamoto, K., and Penner, J. E.: A possible correlation between satellite-derived cloud and aerosol microphysical parameters, Geophysical Research Letters, 28, 1171-1174, 10.1029/2000gl012186, 2001.

Nenes, A., Pandis, S. N., and Pilinis, C.: ISORROPIA: A new thermodynamic equilibrium model for multiphase multicomponent inorganic aerosols, Aquatic Geochemistry, 4, 123-152, 10.1023/a:1009604003981, 1998.

Pandis, S. N. and Seinfeld, J. H.: Mathematical modeling of acid deposition due to radiation fog, Journal of Geophysical Research, 94, 12911-12923, 1989.

Pandis, S. N., Seinfeld, J. H., and Pilinis, C.: Heterogeneous sulfate production in an urban fog, Atmospheric Environment Part a-General Topics, 26, 2509-2522, 10.1016/0960-1686(92)90103-r, 1992.

Seinfeld, J. H. and Pandis, S. N.: Atmospheric Chemistry and Physics: From Air Pollution to Climate Change, 2nd Edn., John Wiley & Sons Inc., New York, 2006.

Schindler, D. W.: Effects of acid-rain on fresh-water ecosystems, Science, 239, 149-157, 10.1126/science.239.4836.149, 1988.

Sun, Y., Wang, Z., Fu, P., Jiang, Q., Yang, T., Li, J., and Ge, X.: The impact of relative humidity on aerosol composition and evolution processes during wintertime in Beijing, China, Atmospheric Environment, 77, 927-934, 2013.

Tian, S. L., Pan, Y. P., and Wang, Y. S.: Size-resolved source apportionment of particulate matter in urban Beijing during haze and non-haze episodes, Atmospheric Chemistry and Physics, 16, 1-19, 10.5194/acp-16-1-2016, 2016.

Wang, G., Zhang, R., Gomez, M. E., Yang, L., Levy, Z. M., Hu, M., Lin, Y., Peng, J., Guo, S., and Meng, J.: Persistent sulfate formation from London Fog to Chinese haze, Proceedings of the National Academy of Sciences of the United States of America, 113, 13630, 2016.

Wang, X. F., Wang, W. X., Yang, L. X., Gao, X. M., Nie, W., Yu, Y. C., Xu, P., Zhou, Y., and Wang, Z.: The secondary formation of inorganic aerosols in the droplet mode through heterogeneous aqueous reactions under haze conditions, Atmospheric Environment, 63, 68-76, 10.1016/j.atmosenv.2012.09.029, 2012.

Wang, Y. X., Zhang, Q. Q., Jiang, J. K., Zhou, W., Wang, B. Y., He, K. B., Duan, F. K., Zhang, Q., Philip, S., and Xie, Y. Y.: Enhanced sulfate formation during China's severe winter haze episode in January 2013 missing from current models, Journal of Geophysical Research-Atmospheres, 119, 16, 10.1002/2013jd021426, 2014.

Wesely, M. L.: Parameterization of surface resistances to gaseous dry deposition in regional-scale numerical models, Atmospheric Environment, 23, 1293-1304, http://dx.doi.org/10.1016/0004-6981(89)90153-4, 1989.

Worsnop, D. R., Zahniser, M. S., Kolb, C. E., Gardner, J. A., Watson, L. R., Vandoren, J. M., Jayne, J. T., and Davidovits, P.: Temperature-dependence of mass accommodation of SO_2 and H_2O_2 on aqueous surfaces, Journal of Physical Chemistry, 93, 1159-1172, 10.1021/j100340a027, 1989.

Xie, Y. N., Ding, A. J., Nie, W., Mao, H. T., Qi, X. M., Huang, X., Xu, Z., Kerminen, V. M., Petaja, T., Chi, X. G., Virkkula, A., Boy, M., Xue, L. K., Guo, J., Sun, J. N., Yang, X. Q., Kulmala, M., and Fu, C. B.: Enhanced sulfate formation by nitrogen dioxide: Implications from in situ observations at the SORPES station, Journal of Geophysical Research-Atmospheres, 120, 12679-12694, 10.1002/2015jd023607, 2015.

Xue, J., Yuan, Z., Griffith, S. M., Yu, X., Lau, A. K. H., and Yu, J. Z.: Sulfate Formation Enhanced by a Cocktail of High NOx, SO2, Particulate Matter, and Droplet pH during Haze-Fog Events in Megacities in China: An Observation-Based Modeling Investigation, Environmental Science & Technology, 50(14), 7325-7334, 2016.

Zheng, G. J., Duan, F. K., Su, H., Ma, Y. L., Cheng, Y., Zheng, B., Zhang, Q., Huang, T., Kimoto, T., Chang, D., Pöschl, U., Cheng, Y. F., and He, K. B.: Exploring the severe winter haze in Beijing: the impact of synoptic weather, regional transport and heterogeneous reactions, Atmospheric Chemistry and Physics, 15, 2969-2983, 2015.

Zhang, Q., Streets, D. G., Carmichael, G. R., He, K. B., Huo, H., Kannari, A., Klimont, Z., Park, I. S., Reddy, S., Fu, J. S., Chen, D., Duan, L., Lei, Y., Wang, L. T., and Yao, Z. L.: Asian emissions in 2006 for the NASA INTEX-B mission, Atmospheric Chemistry and Physics, 9, 5131-5153, 2009.

Zhang, R., Leu, M. T., and Keyser, L. F.: Hydrolysis of N_2O_5 and $ClONO_2$ on the $H_2SO_4/HNO_3/H_2O$ ternary solutions under stratospheric conditions, Geophysical Research Letters, 22, 1493-1496, 1995.

Zhang, R. Y., Wang, G. H., Guo, S., Zarnora, M. L., Ying, Q., Lin, Y., Wang, W. G., Hu, M., and Wang, Y.: Formation of Urban Fine Particulate Matter, Chemical Reviews, 115, 3803-3855, 10.1021/acs.chemrev.5b00067, 2015.

Zhao, J., Levitt, N. P., Zhang, R., and Chen, J.: Heterogeneous reactions of methylglyoxal in acidic media: implications for secondary organic aerosol formation, Environmental Science & Technology, 40, 7682-7687, 2006.

Figure Captions

Figure 1 WRF-CHEM simulation domains with topography for (a) the Guanzhong basin and (b) Beijing-Tianjin-Hebei. The black squares represent ambient monitoring sites. The red filled circles in (a) and (b) denote the deployment locations of the HR-ToF-AMS in Xi'an and Beijing, respectively.

Figure 2 Scatter plot of the observed sulfate with $PM_{2.5}$ mass concentrations at IEECAS site in Xi'an during the wintertime from 2003 to 2011.

Figure 3 Average O_3 mass concentrations over monitoring sites in GZB as a function of the $PM_{2.5}$ mass concentration during the wintertime from 2013 to 2015.

Figure 4 Scatter plot of the observed relative humidity with sulfate mass concentrations at IEECAS site in Xi'an during the wintertime from 2003 to 2011.

Figure 5 Scatter plot of the observed $PM_{2.5}$ with iron mass concentrations at IEECAS site in Xi'an during the wintertime from 2003 to 2011.

Figure 6 Sulfate growth simulated by the box model with the $HRSO_2$ parameterization under various relative humidity conditions at IEECAS site in Xi'an from 07:30 to 09:30 BJT on December 23, 2013. The black dots denote the HR-ToF-AMS measurement and the solid lines with different colors represent the box model simulations under different relative humidity.

Figure 7 Pattern comparison of simulated vs. observed near-surface $PM_{2.5}$ at 00:00 BJT during the selected six days in GZB from 16 to 27 December 2013. Colored circles: $PM_{2.5}$ observations; color contour: $PM_{2.5}$ simulations in the E-case; black arrows: simulated surface winds in the E-case.

Figure 8 Same as Figure 7, but in BTH from 13 to 21 January 2014.

Figure 9 Comparison of measured and predicted diurnal profiles of near-surface hourly (a) NO_2 and (b) SO_2 averaged over all ambient monitoring sites in GZB from 16 to 27 December 2013. The black dots correspond to the observations, and the solid red and blue lines are the simulations in the E-case and B-case, respectively.

Figure 10 Same as Figure 9, but in BTH from 13 to 21 January 2014.

Figure 11 Comparison of measured and simulated diurnal profiles of inorganic aerosols of (a) sulfate, (b) nitrate, and (c) ammonium in Xi'an from 16 to 27 December 2013. The black dots represent the observations, and the solid red and blue lines denote the simulations in the E-case and B-case, respectively.

Figure 12 Same as Figure 11, but in Beijing from 13 to 21 January 2014.

Figure 13 Comparison of measured (black dots) and simulated (blue lines, in the E-case) diurnal profiles of the relative humidity (a) in Xi'an from 16 to 27 December 2013 and (b) in Beijing from 13 to 21 January 2014.

Figure 14 Observed and simulated diurnal cycles of mass concentrations of NO_2 and SO_2 averaged over GZB and BTH and the sulfate, nitrate, and ammonium aerosols in Xi'an and Beijing during the simulated episodes.

Figure 15 Comparison of measured and predicted diurnal profiles of near-surface hourly $PM_{2.5}$ mass concentration averaged over all ambient monitoring stations (a) in GZB from 16 to 27 December 2013 and (b) in BTH from 13 to 21 January 2014. The black dots represent the observations, and the solid red and blue lines are the simulations in the E-case and B-case, respectively.

Figure 16 Distribution of the average near-surface $PM_{2.5}$ contribution due to the SO_2 heterogeneous reactions in GZB and BTH during the simulated episodes.

Figure 17 Average (a) sulfate, (b) nitrate, (c) ammonium, and (d) $PM_{2.5}$ mass concentrations in GZB during the simulation period as a function of the sulfate mass concentration in the E-case. The red and blue dots represent average mass concentrations in the E-case and B-case, respectively.

Figure 18 Same as Figure 16, but in BTH from 13 to 21 January 2014.

Table 1 WRF-CHEM model configurations and observation sites

Regions	**Guanzhong Basin (GZB)**	**Beijing-Tianjin-Hebei (BTH)**
Simulation period	December 16 to 27, 2013	January 13 to 21, 2014
Domain size	150 × 150	
Domain center	34.25°N, 109°E	39°N, 117°E
Horizontal resolution	6km × 6km	
Vertical resolution	35 vertical levels with a stretched vertical grid with spacing ranging from 30 m near the surface, to 500 m at 2.5 km and 1 km above 14 km	
Microphysics scheme	WSM 6-class graupel scheme (Hong and Lim, 2006)	
Boundary layer scheme	MYJ TKE scheme (Janjić, 2002)	
Surface layer scheme	MYJ surface scheme (Janjić, 2002)	
Land-surface scheme	Unified Noah land-surface model (Chen and Dudhia, 2001)	
Longwave radiation scheme	Goddard longwave scheme (Chou and Suarez, 2001)	
Shortwave radiation scheme	Goddard shortwave scheme (Chou and Suarez, 1999)	
Meteorological boundary and initial conditions	NCEP 1°×1° reanalysis data	
Chemical initial and boundary conditions	MOZART 6-hour output (Horowitz et al., 2003)	
Anthropogenic emission inventory	Developed by Zhang et al. (2009)	
Biogenic emission inventory	MEGAN model developed by Guenther et al. (2006)	
Aerosol Observation Sites		
City	Xi’an	Beijing
Longitude and latitude	34.23°N, 108.88°E	40.00°N, 116.38°E

Table 2 Box model configurations

Time (BJT)	07:00 – 08:00	08:00 – 09:00	09:00 – 10:00
Temperature (^oC)	-3.7	-3.2	-2.1
SO_2 concentration ($\mu g\ m^{-3}$)	10.7	10.4	25.5
Nitrate concentration ($\mu g\ m^{-3}$)*	67.6	70.1	69.1
Ammonium concentration ($\mu g\ m^{-3}$) *	65.2	76.0	91.9

*The HR-ToF-AMS measures sulfate, nitrate, and ammonium aerosols with a time resolution of 1 minute. The high temporal resolution nitrate and ammonium are used to constrain the box model and the hourly average is presented in the table.

Table 3 Statistical comparisons of simulated and measured sulfate, nitrate, and ammonium concentrations in Xi'an and Beijing

City	Species	E-case		B-case	
		MB (μg m^{-3})	*IOA*	*MB* (μg m^{-3})	*IOA*
Xi'an	Sulfate	-17.0	0.89	-72.4	0.50
	Nitrate	-13.4	0.83	-6.3	0.86
	Ammonium	-5.1	0.92	-20.1	0.72
Beijing	Sulfate	-0.8	0.88	-8.4	0.65
	Nitrate	-4.2	0.88	-1.9	0.92
	Ammonium	-2.7	0.89	-4.1	0.87

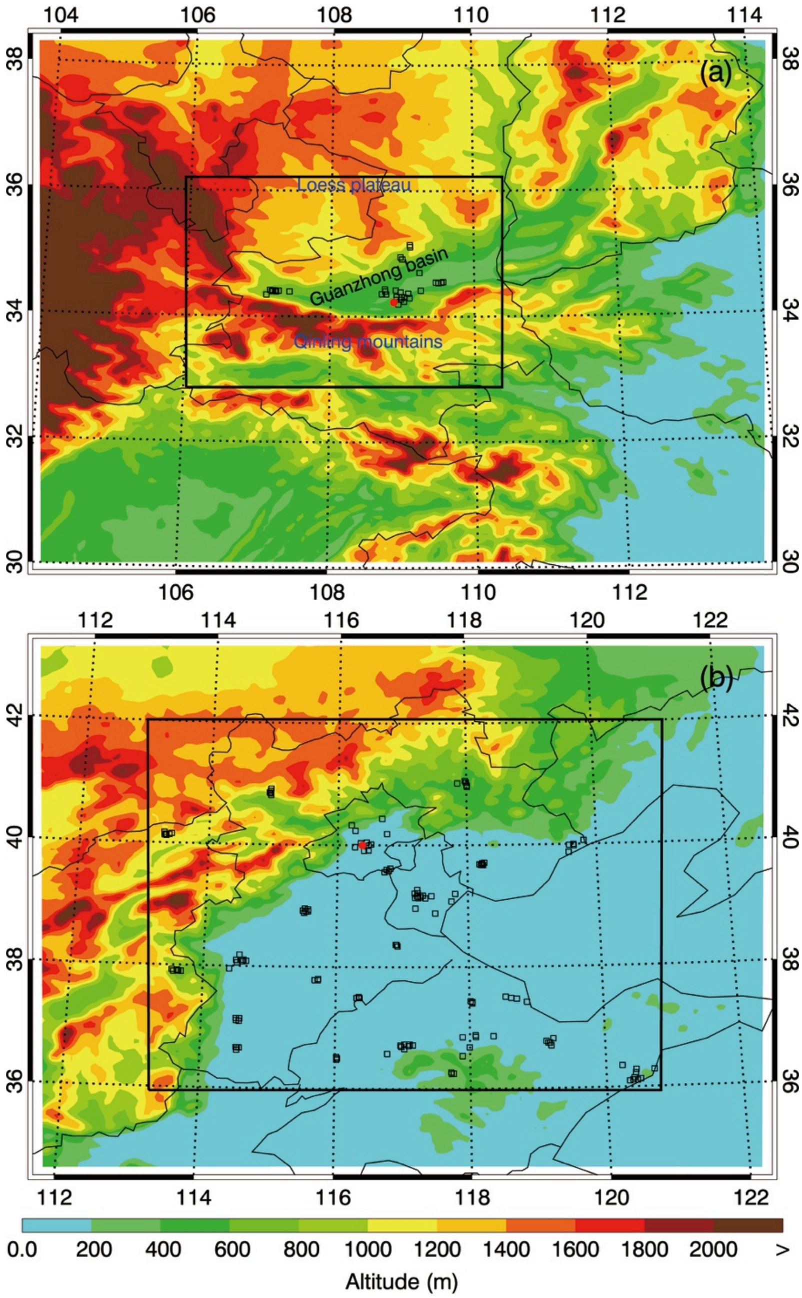

Figure 1 WRF-CHEM simulation domains with topography for (a) the Guanzhong basin and (b) Beijing-Tianjin-Hebei. The black squares represent ambient monitoring sites. The red filled circles in (a) and (b) denote the deployment locations of the HR-ToF-AMS in Xi’an and Beijing, respectively.

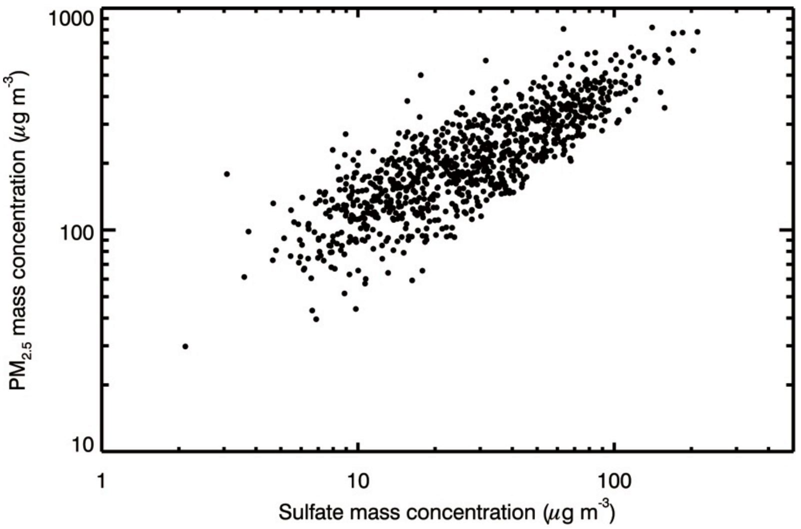

Figure 2 Scatter plot of the observed sulfate with $PM_{2.5}$ mass concentrations at IEECAS site in Xi'an during the wintertime from 2003 to 2011.

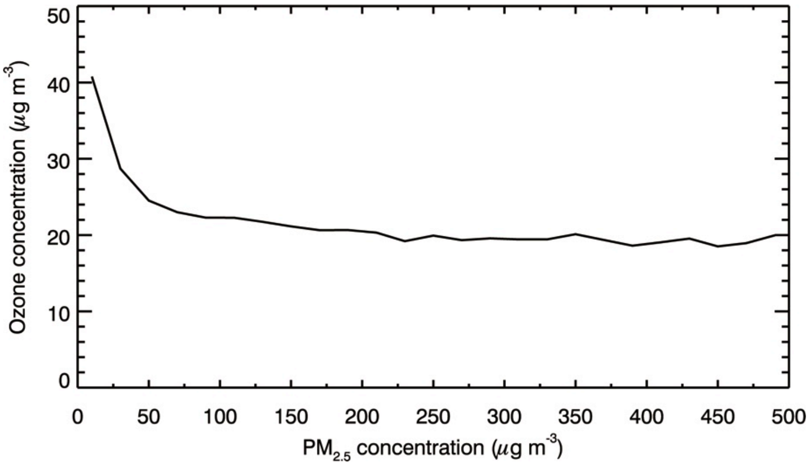

Figure 3 Average O_3 mass concentrations over monitoring sites in GZB as a function of the $PM_{2.5}$ mass concentration during the wintertime from 2013 to 2015.

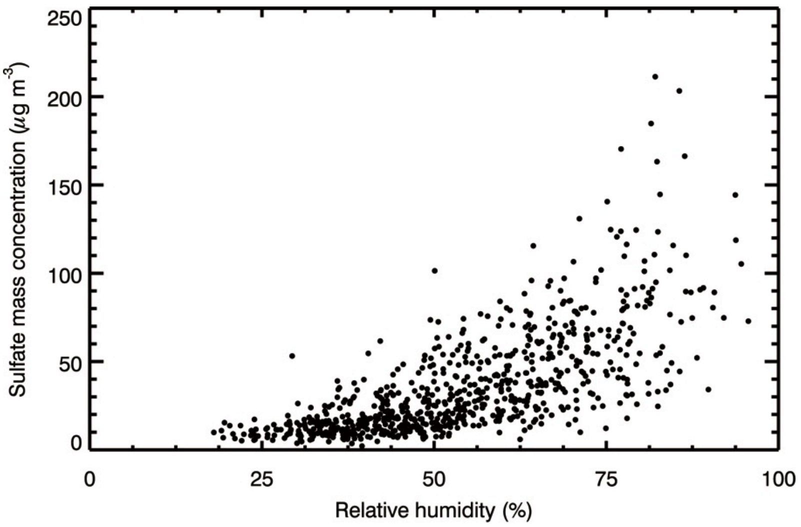

Figure 4 Scatter plot of the observed relative humidity with sulfate mass concentrations at IEECAS site in Xi’an during the wintertime from 2003 to 2011.

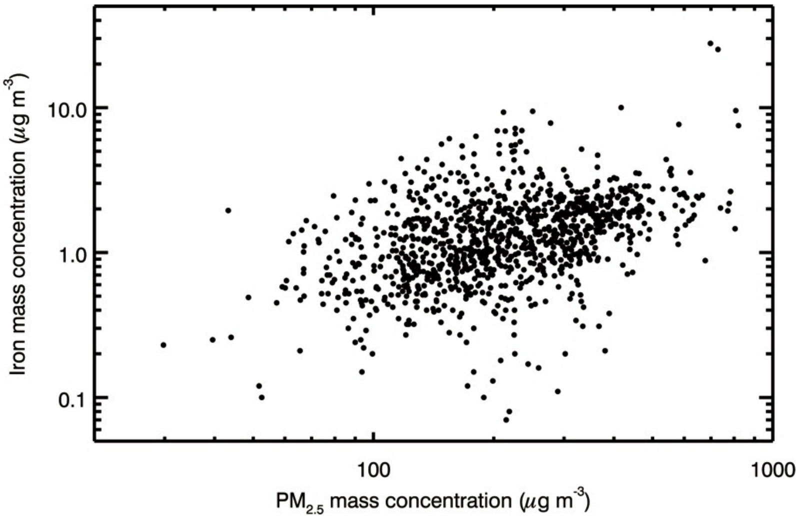

Figure 5 Scatter plot of the observed $PM_{2.5}$ with iron mass concentrations at IEECAS site in Xi’an during the wintertime from 2003 to 2011.

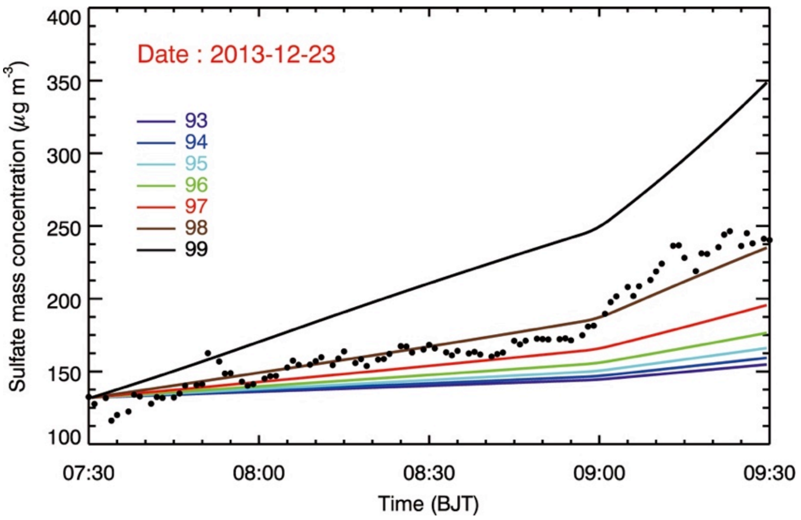

Figure 6 Sulfate growth simulated by the box model with the HRSO$_2$ parameterization under various relative humidity at IEECAS site in Xi'an from 07:30 to 09:30 BJT on December 23, 2013. The black dots denote the HR-ToF-AMS measurement and the solid lines with different colors represent the box model simulations under different relative humidity.

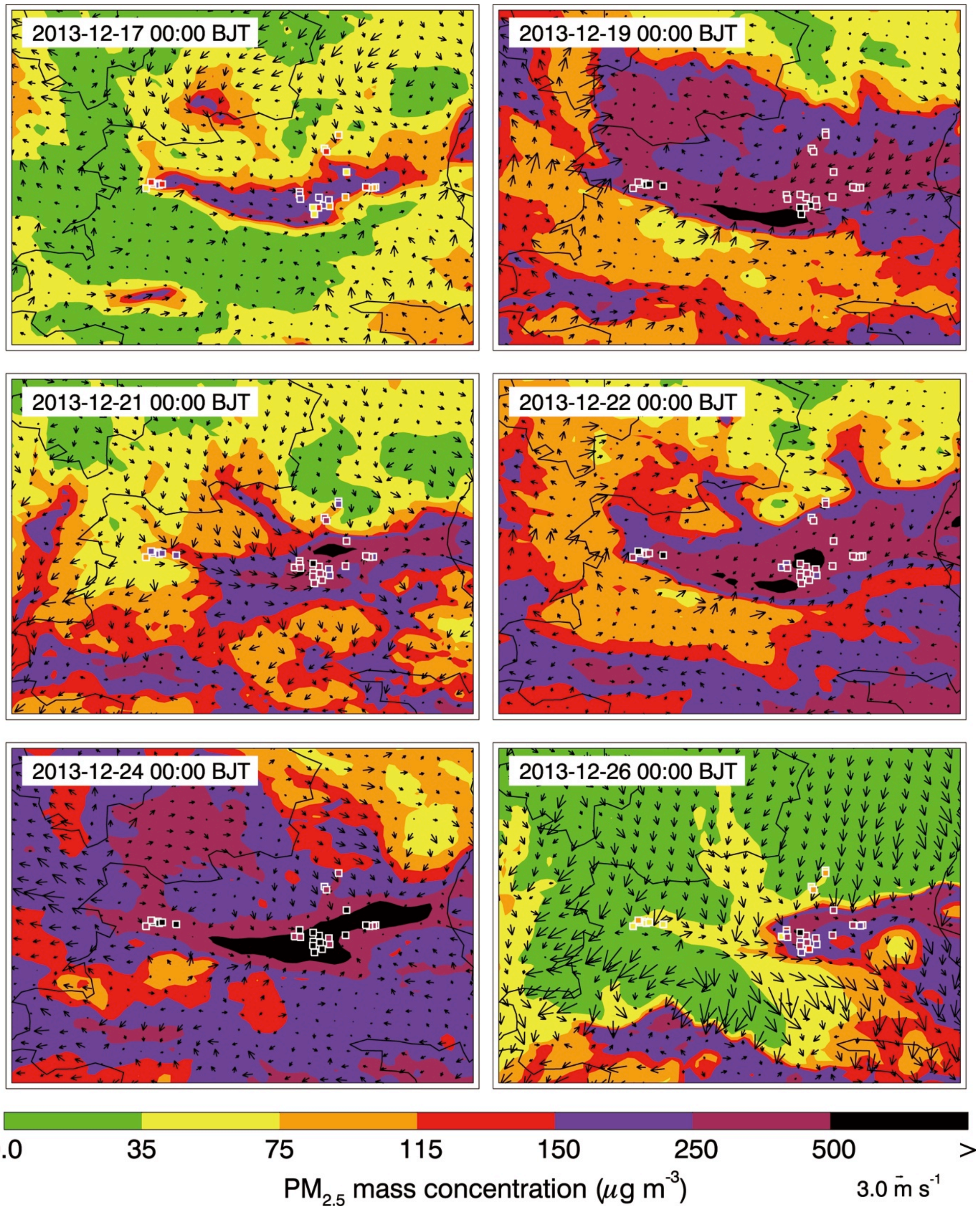

Figure 7 Pattern comparison of simulated vs. observed near-surface $PM_{2.5}$ at 00:00 BJT on the selected six days in GZB from 16 to 27 December 2013. Colored circles: $PM_{2.5}$ observations; color contour: $PM_{2.5}$ simulations in the E-case; black arrows: simulated surface winds in the E-case.

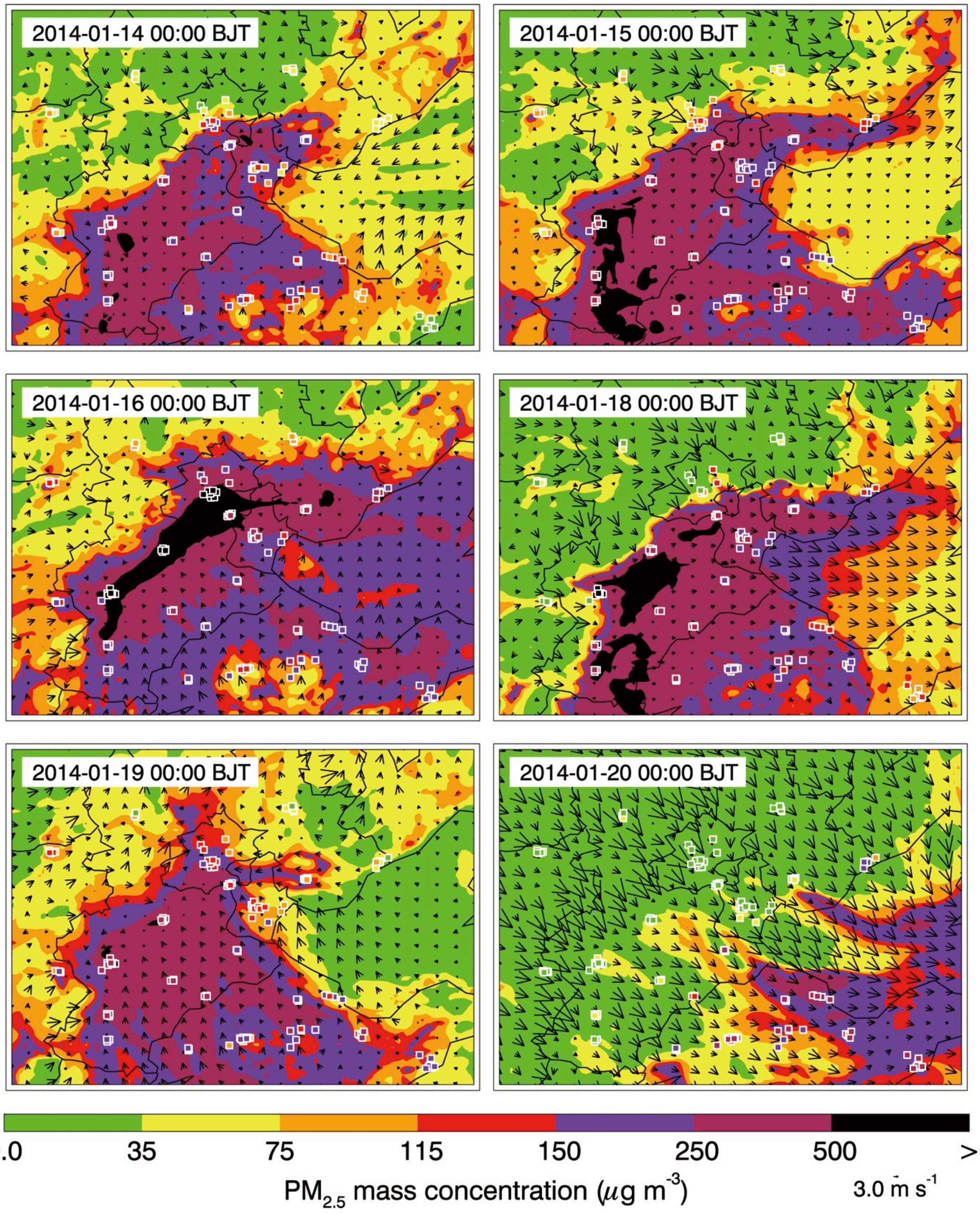

Figure 8 Same as Figure 7, but in BTH from 13 to 21 January 2014.

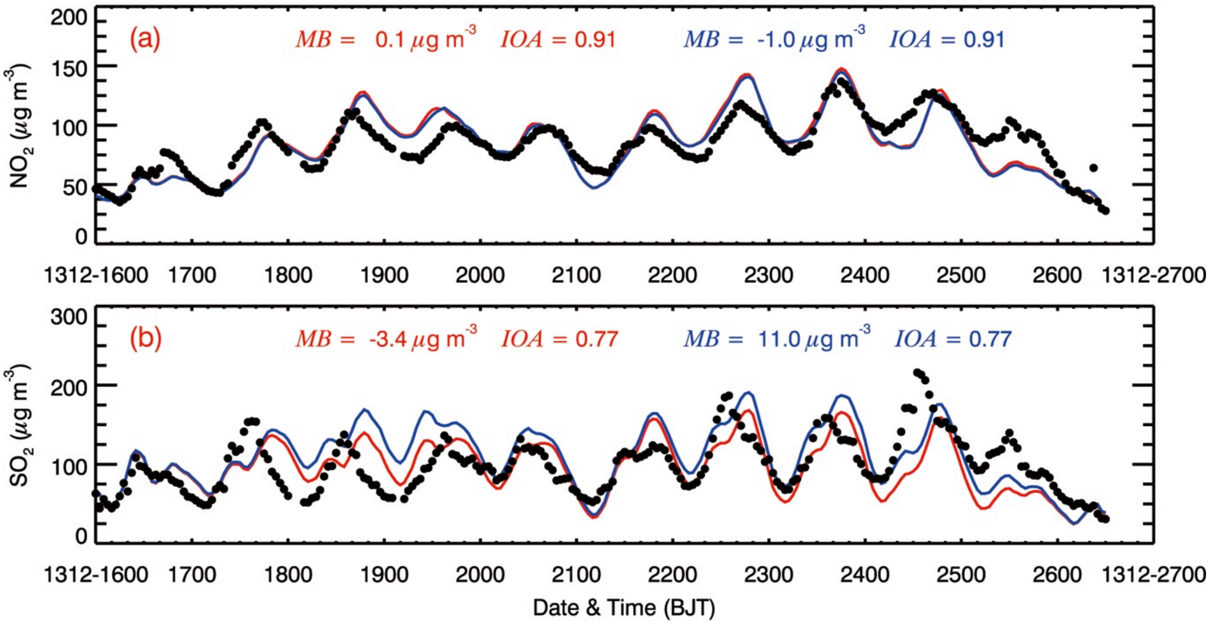

Figure 9 Comparison of measured and predicted diurnal profiles of near-surface hourly (a) NO$_2$ and (b) SO$_2$ averaged over all ambient monitoring sites in GZB from 16 to 27 December 2013. The black dots correspond to the observations, and the solid red and blue lines are the simulations in the E-case and B-case, respectively. The x-axis labels (named date and time) represent year, month, day and hour (YYMM-DDHH) or day and hour (DDHH). For example, 1312-1600 represents 00 BJT on 16 December 2013.

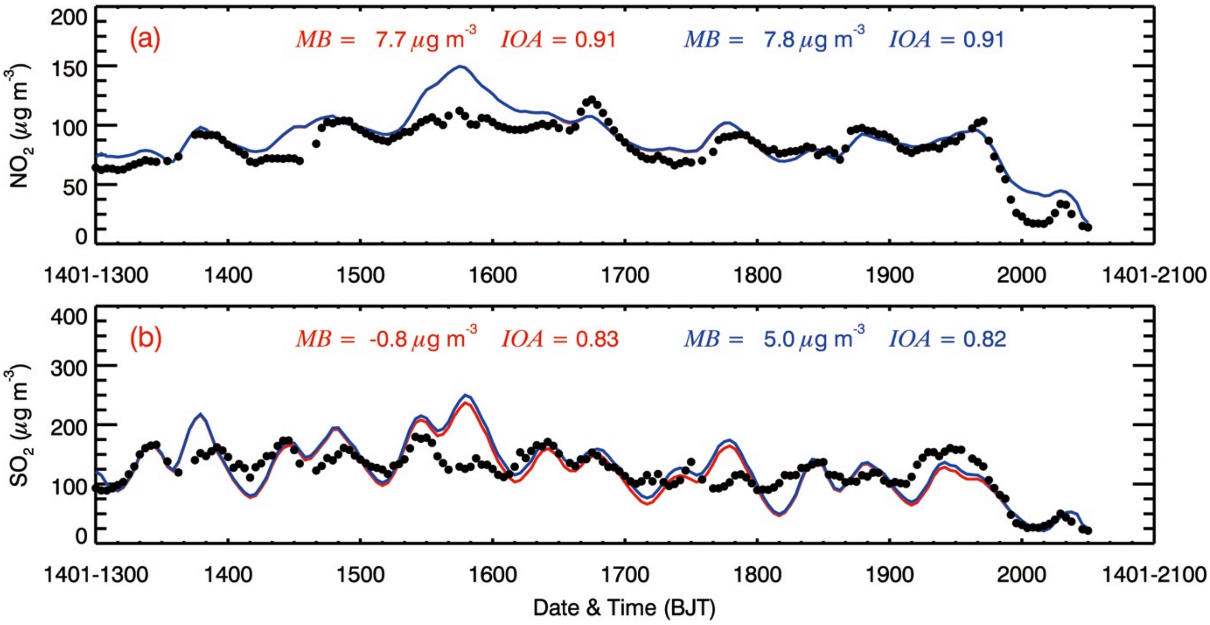

Figure 10 Same as Figure 9, but in BTH from 13 to 21 January 2014.

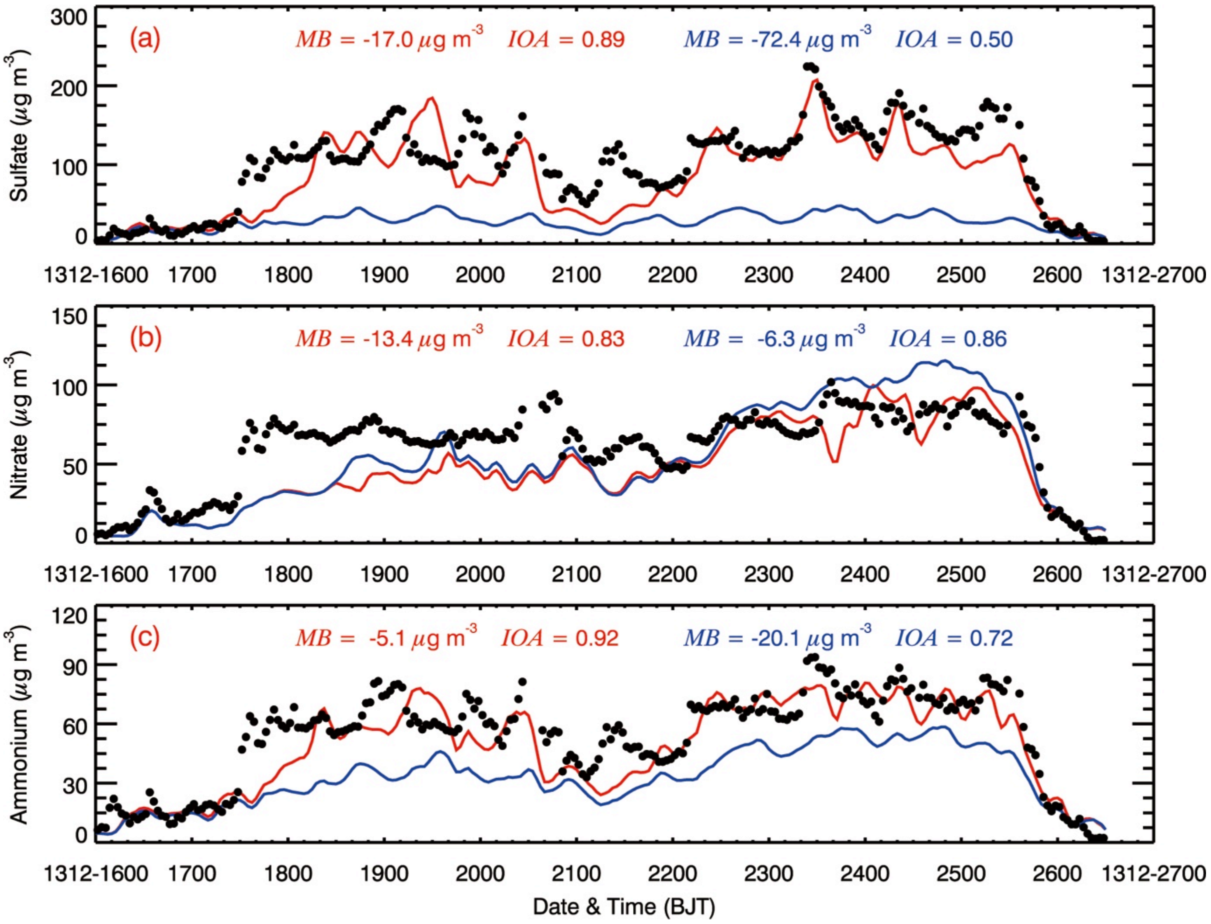

Figure 11 Comparison of measured and simulated diurnal profiles of inorganic aerosols of (a) sulfate, (b) nitrate, and (c) ammonium in Xi'an from 16 to 27 December 2013. The black dots represent the observations, and the solid red and blue lines denote the simulations in the E-case and B-case, respectively.

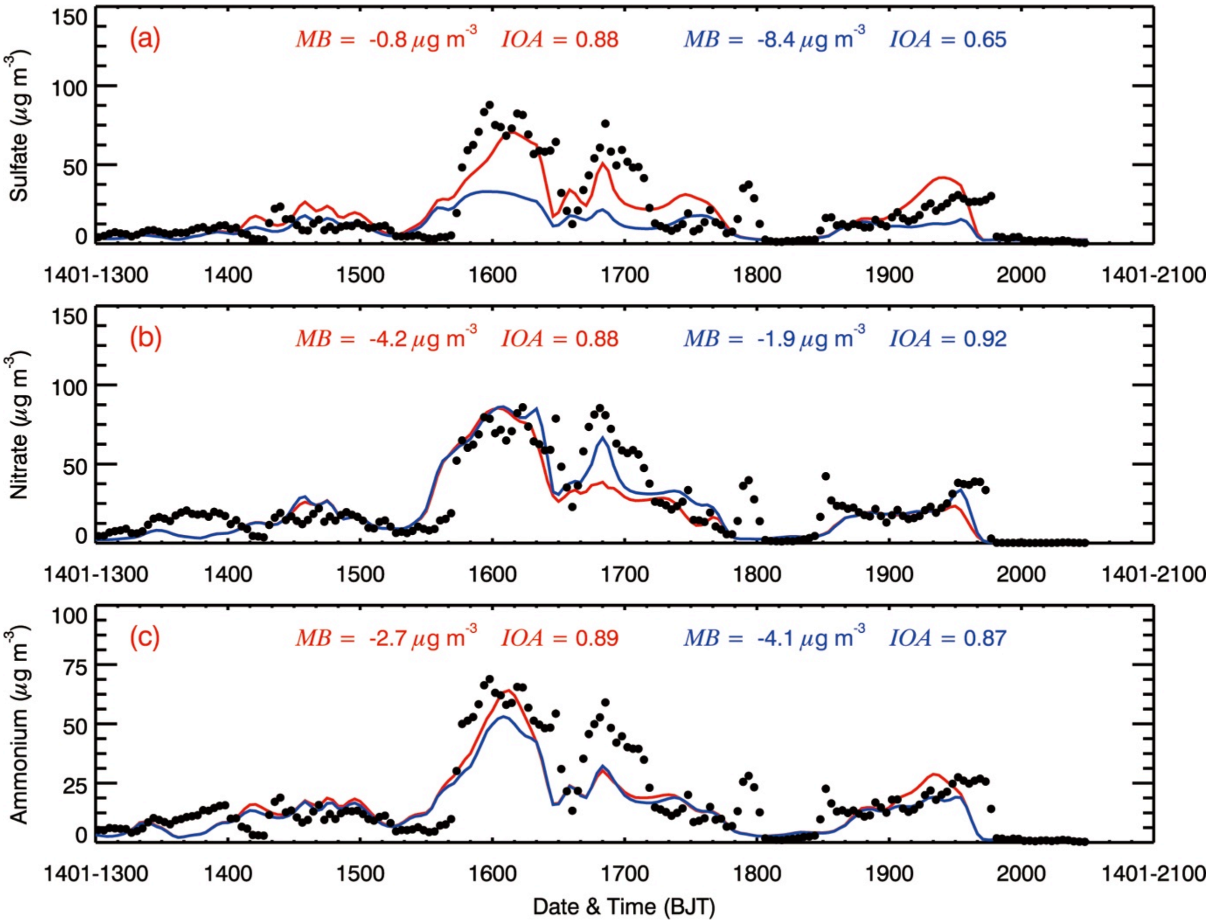

Figure 12 Same as Figure 11, but in Beijing from 13 to 21 January 2014.

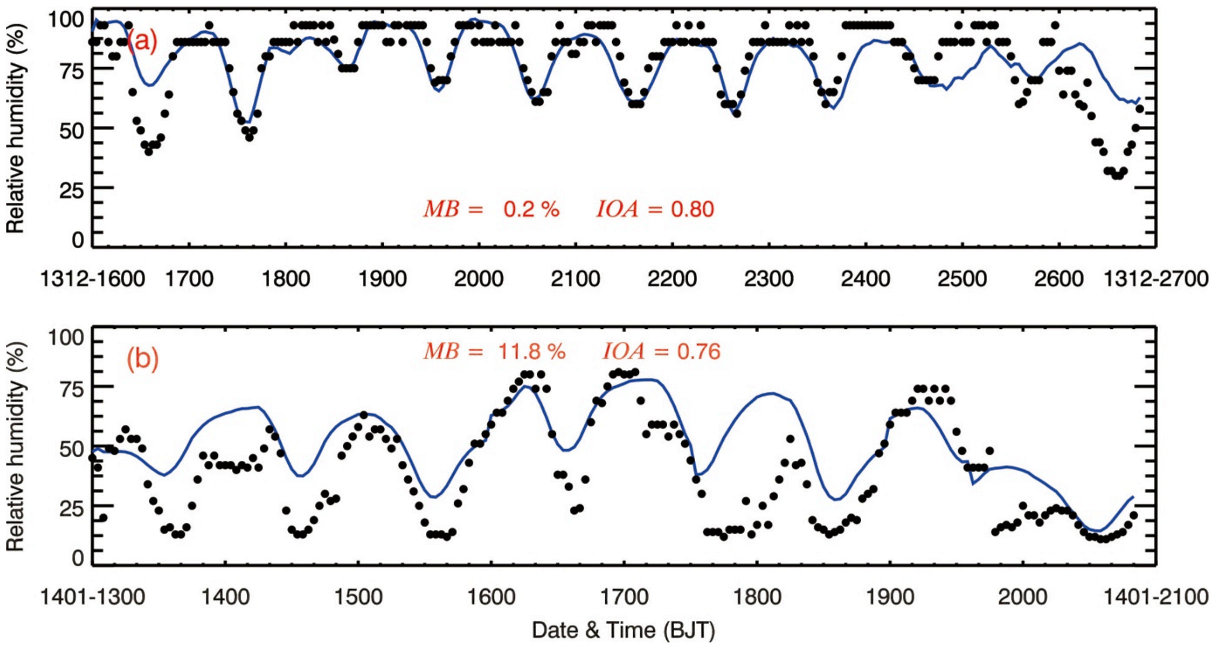

Figure 13 Comparison of measured (black dots) and simulated (blue lines, in the E-case) diurnal profiles of the relative humidity (a) in Xi'an from 16 to 27 December 2013 and (b) in Beijing from 13 to 21 January 2014.

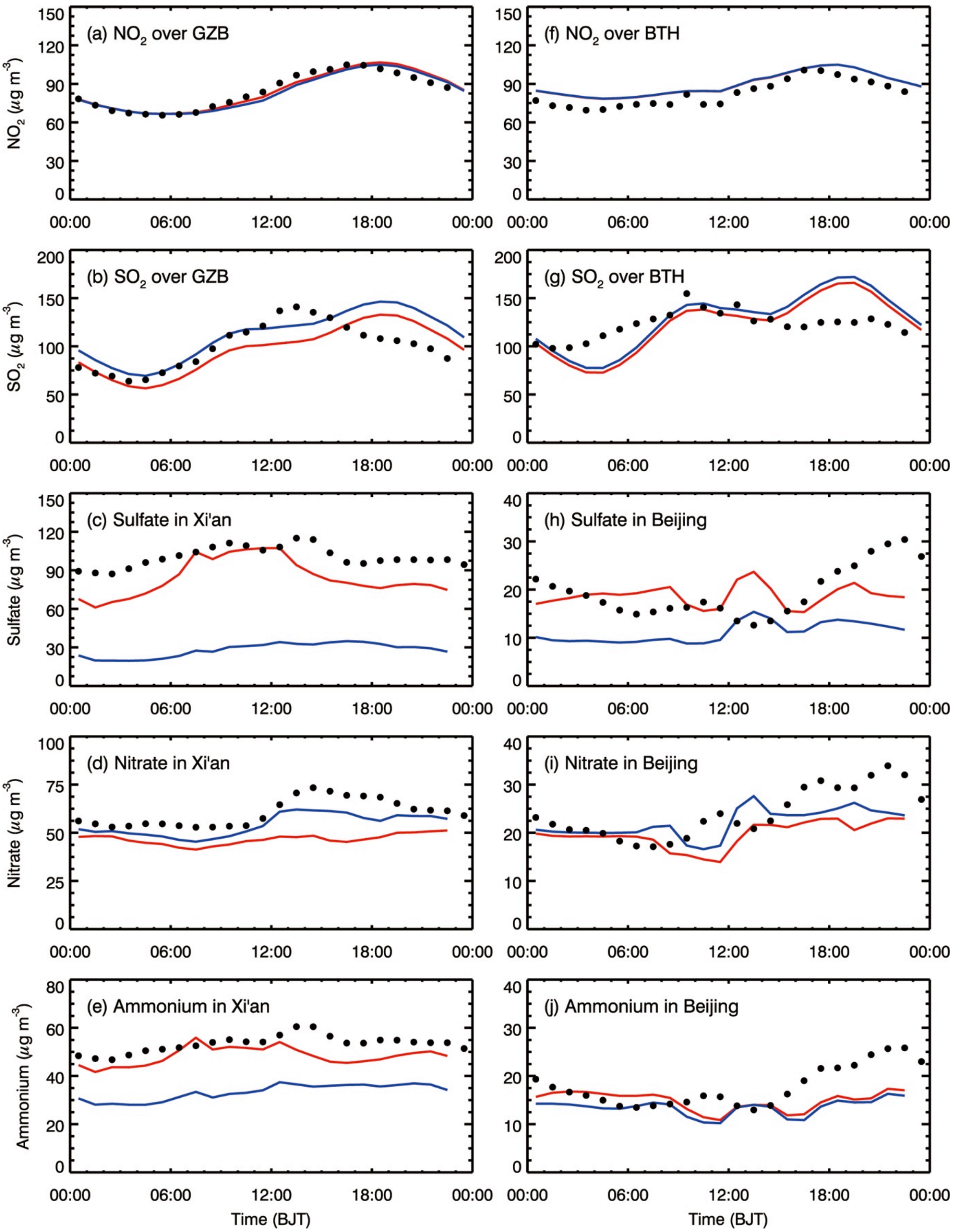

Figure 14 Observed and simulated diurnal cycles of mass concentrations of NO$_2$ and SO$_2$ averaged over GZB and BTH and the sulfate, nitrate, and ammonium aerosols in Xi’an and Beijing during the simulated episodes.

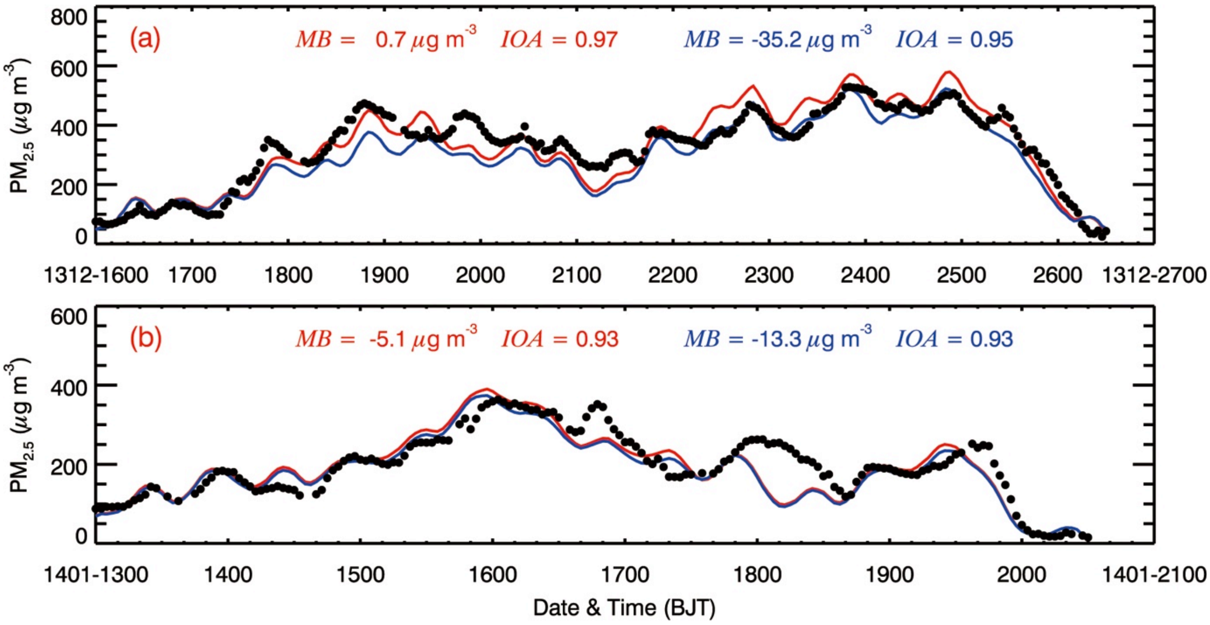

Figure 15 Comparison of measured and predicted diurnal profiles of near-surface hourly $PM_{2.5}$ mass concentration averaged over all ambient monitoring stations (a) in GZB from 16 to 27 December 2013 and (b) in BTH from 13 to 21 January 2014. The black dots represent the observations, and the solid red and blue lines are the simulations in the E-case and B-case, respectively.

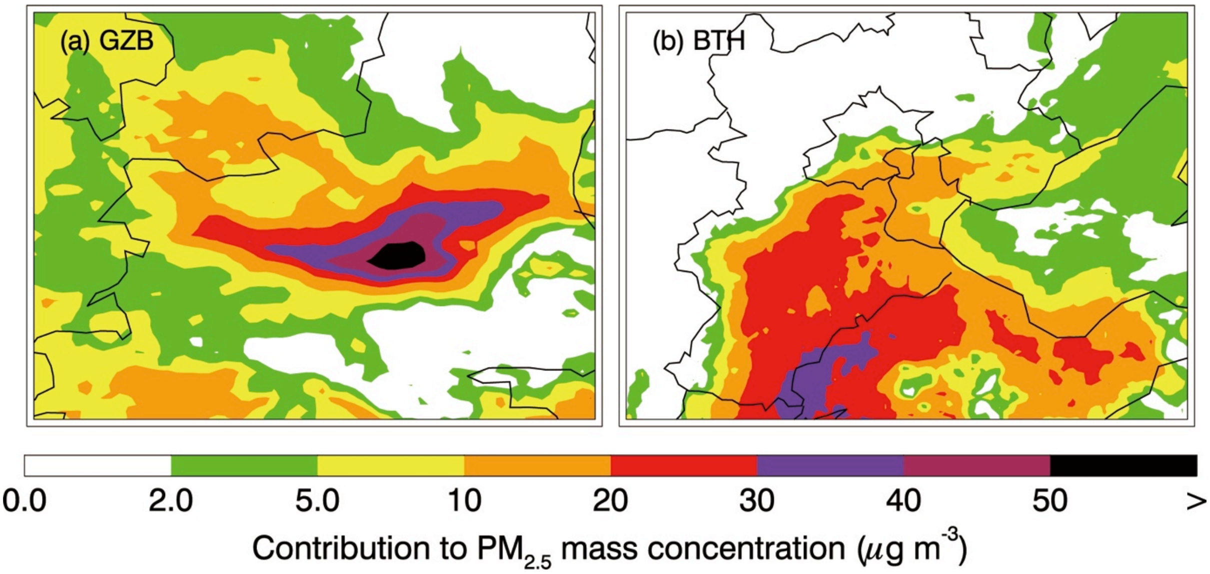

Figure 16 Distribution of the average near-surface $PM_{2.5}$ contribution due to the SO_2 heterogeneous reactions in GZB and BTH during the simulated episodes.

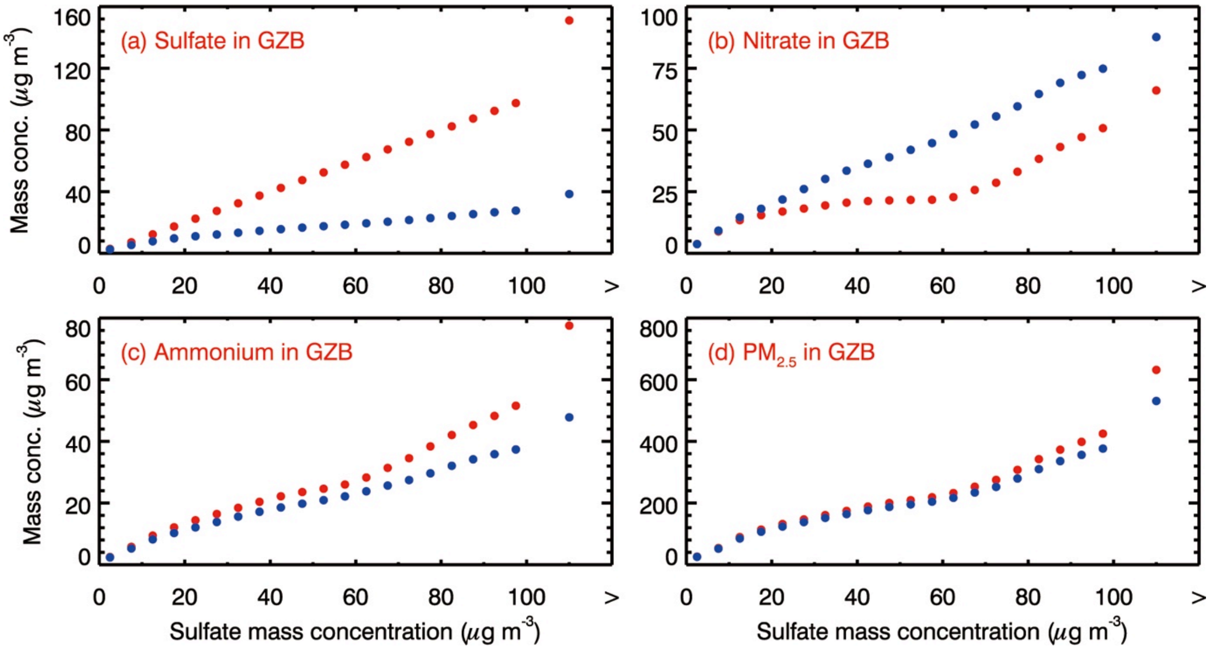

Figure 17 Average (a) sulfate, (b) nitrate, (c) ammonium, and (d) $PM_{2.5}$ mass concentrations in GZB during the simulation period as a function of the sulfate mass concentration in the E-case. The red and blue dots represent average mass concentrations in the E-case and B-case, respectively.

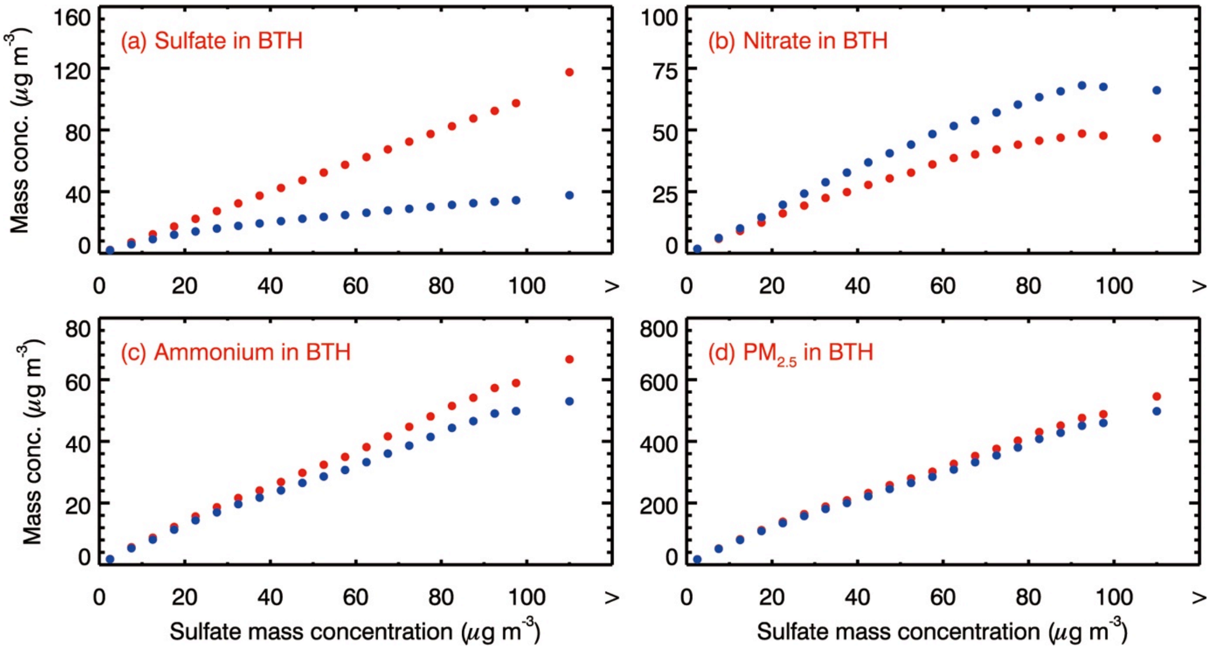

Figure 18 Same as Figure 16, but in BTH from 13 to 21 January 2014.